C S P

The DOE Center of Excellence for the Synthesis and Processing of Advanced Materials

BASIC ENERGY SCIENCES
DIVISION OF MATERIALS SCIENCE

Member Laboratories: Ames Laboratory, Argonne National Laboratory, Brookhaven National Laboratory, Idaho National Engineering and Environmental Laboratory, University of Illinois Frederick Seitz Materials Research Laboratory, Lawrence Berkeley National Laboratory, Lawrence Livermore National Laboratory, Los Alamos National Laboratory, National Renewable Energy Laboratory, Oak Ridge National Laboratory, Pacific Northwest National Laboratory, Sandia National Laboratories

Research Briefs

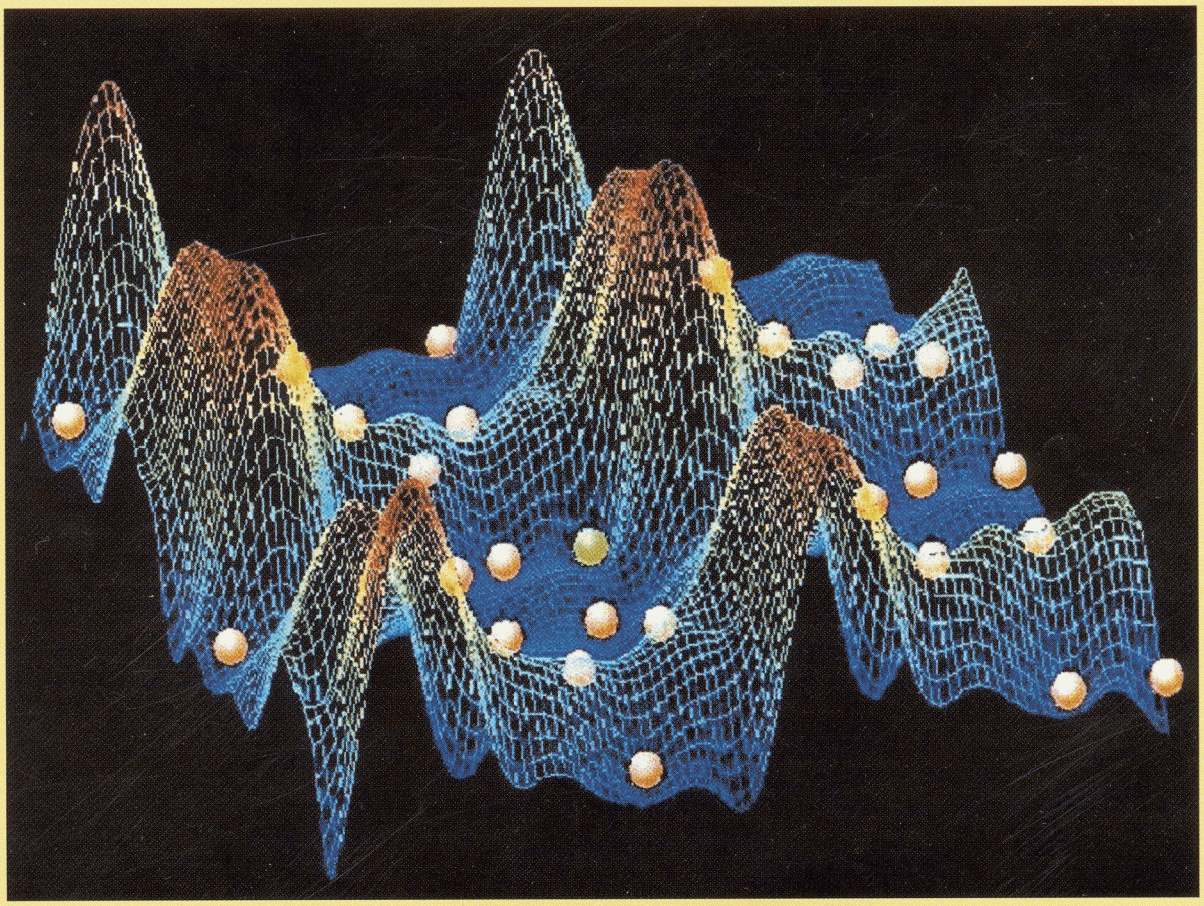

For questions and additional information contact:

George A. Samara
Sandia National Laboratories/NM
Phone: (505) 844-6653
Fax: (505) 844-4045
E-mail: gasamar@sandia.gov

C S P

The DOE **C**enter of Excellence for the
Synthesis and **P**rocessing
of Advanced Materials

BASIC ENERGY SCIENCES
DIVISION OF MATERIALS SCIENCE

Research Briefs

May 1999

Table of Contents

Research Briefs

Table of Contents

Preface

This publication, Research Briefs, is designed to inform present and potential customers and partners of the DOE Center of Excellence for the Synthesis and Processing of Advanced Materials (CSP) about significant advances resulting from Center-coordinated research. The format for Research Briefs is an easy-to-read, not highly technical, concise presentation of the accomplishments. Each Brief provides a statement of the motivation for the research followed by a description of the accomplishment and its significance.

The Center is a distributed center for promoting coordinated, collaborative research partnerships related to the synthesis and processing of advanced materials. It was established by the Department of Energy's Division of Materials Sciences, Office of Basic Energy Sciences and the DOE Laboratories in recognition of the enabling role of materials synthesis and processing to numerous materials fabrication- and manufacturing-intensive technologies. The participants include investigators from 12 DOE national laboratories, universities and the private sector. The Center has a technology perspective provided by a Technology Steering Group.

By bringing together synergistic activities and capabilities in selected focus areas of materials synthesis and processing, the Center's goal is to be a vehicle for providing added value and making impact. The Center is also allowing better coordinated strategic planning by the Division of Materials Sciences and the Laboratories and faster response time to special needs and opportunities. Additionally, the Center strives to be a model of R and D integration within the Department of Energy as well as a model of cooperation among the participating institutions.

The overall objective of the Center is,
To enhance the science and engineering of materials synthesis and processing in order to meet the programmatic needs of the Department of Energy and to facilitate the technological exploitation of materials.

Synthesis and processing (S&P) are those essential elements of Materials Science and Engineering (MS&E) that deal with (1) the assembly of atoms or molecules to form materials, (2) the manipulation and control of the structure at all levels from the atomic to the macroscopic scale, and (3) the development of processes to produce materials for specific applications. Clearly, S&P represent a

large area of MS&E that spans the range from fundamental research to technology. The goal of basic research in this area ranges from the creation of new materials and the improvement of the properties of known materials, to the understanding of such phenomena as diffusion, crystal growth, sintering, phase transitions, to the development of novel diagnostic, modeling and processing approaches, etc. On the applied side, the goal of S&P is to translate scientific results into useful materials by developing processes capable of producing high quality cost-effective products.

The technical emphasis of the Center has been on eight focused multilaboratory projects which draw on the complementary strengths of the member institutions in their ongoing research programs. These projects were selected on the basis of the following criteria:

- scientific excellence
- clear relationship to energy technologies
- involvement of several laboratories
- existing or potential partnerships with DOE Technologies-funded programs
- existing or potential "in-kind" partnerships with industry

Each Project is coordinated by a knowledgeable representative from one of the participating laboratories. The Projects and their Coordinators are listed in the accompanying table. In this issue of Research Briefs we have selected a few accomplishments from each of the Projects. An Executive Summary provides highlights of these accomplishments organized by Project. Readers are encouraged to contact any of the Coordinators for information about the Center and its accomplishments.

George A. Samara
May 1999

The Center's Member Laboratories

The member laboratories of the Center are:

- Ames Laboratory (Ames)
- Argonne National Laboratory (ANL)
- Brookhaven National Laboratory (BNL)
- Idaho National Engineering and Environmental Laboratory (INEEL)
- University of Illinois Frederick Seitz Materials Research Laboratory (UI/MRL)
- Lawrence Berkeley National Laboratory (LBNL)
- Lawrence Livermore National Laboratory (LLNL)
- Los Alamos National Laboratory (LANL)
- National Renewable Energy Laboratory (NREL)
- Oak Ridge National Laboratory (ORNL)
- Pacific Northwest National Laboratory (PNNL)
- Sandia National Laboratories (SNL)

Membership of the Technology Steering Group

Member	Affiliation
Dr. Thomas C. Clarke	IBM-Almaden
Dr. Howard Feibus*	DOE/Fossil Energy
Dr. David W. Johnson, Jr.	Bell Labs, Lucent Technologies
Dr. Hylan B. Lyon	Marlow Industries
Dr. Neil E. Paton	Howmet Research Corporation
Dr. Charles Sorrell	DOE/Energy Efficiency & Renewable Energy
Dr. John Stringer	Electric Power Research Institute (EPRI)

*recently retired

Center Projects and Their Coordinators

Project	Coordinator(s)
Metal Forming	Michael Kassner (Oregon State) Phone: (541) 737-7023 FAX: (541) 737-2600 E-mail: kassner@engr.orst.edu
Materials Joining	R. Bruce Thompson (Ames) Phone: (515) 294-9649 FAX: (515) 294-4456 E-mail: thompsonrb@ameslab.gov
Microstructural Engineering with Polymers	Gregory J. Exarhos (PNNL) Phone: (509) 375-2440 FAX: (509) 375-2186 E-mail: gj_exarhos@pnl.gov
Tailored Microstructures in Hard Magnets	Bob Dunlap (ANL) Phone: (708) 252-4925 FAX: (708) 252-4798 E-mail: bddunlap@anl.gov
Processing for Surface Hardness	James B. Roberto (ORNL) Phone: (423) 576-0227 FAX: (423) 574-4143 E-mail: jlr@ornl.gov
Mechanically Reliable Surface Oxides for High-Temperature Corrosion Resistance	Linda L. Horton (ORNL) Phone: (423) 574-5081 FAX: (423) 574-7659 E-mail: hortonll@ma160.ms.ornl.gov
High Efficiency Photovoltaics	Satyen Deb (NREL) Phone: (303) 384-6405 FAX: (303) 384-6481 E-mail: satyen_deb@nrel.gov
Design and Synthesis of Ultrahigh-Temperature Intermetallics	Roddie R. Judkins (ORNL) Phone: (423) 574-4572 FAX: (423) 574-5812 E-mail: judkinsrr@ornl.gov and R. Bruce Thompson (Ames) Phone: (515) 294-9649 Fax: (515) 294-4456 E-mail: thompsonrb@cnde.iastate.edu
Overall Center Coordinator	George A. Samara (SNL/NM) Phone: (505) 844-6653 FAX: (505) 844-4045 E-mail: gasamar@sandia.gov

Executive Summary

The *Research Briefs* presented in this publication are intended to inform the Center's present and potential customers and partners about significant advances resulting from Center-coordinated research. Selected accomplishments from each of the Center's focused projects are presented. This Executive Summary states the overall objective of each project followed by highlights of the accomplishments presented later in more detail.

Metal Forming

Objective

Develop a scientific understanding of the phenomena relating to the forming of aluminum alloys for industrial (especially automotive) applications.

Highlights

- Mechanical properties and texture measurements as well as microstructural characterization were employed to understand the large changes that occur during the forming of aluminum alloy 5182. The work identified (011) octahedral slip (in addition to the usual (111) slip) as responsible for the bimodal texture observed at high temperatures and low strain rates. This non-classical slip system has to be invoked to accurately model texture development during hot rolling.

- TEM observations of the dislocation structures in a number of fcc metals and alloys have strengthened our earlier finding that there exist scaling relationships for the misorientations and spacings of grain boundaries which indicate that the deformation structure and its evolution are governed by relatively simple laws for the collective properties of dislocation microstructures produced by plastic deformation.

- Studies of the superplastic alloy Al-6Mg-03Sc have led to better understanding of the role of fine Al_3Sc particle precipitates in the recrystallization and deformation behavior of this alloy and to the ability to tailor its mechanical properties. In a complementary effort it was demonstrated that semi-solids can be produced exclusively by thermal treatments, providing a novel and inexpensive alternative to conventional Al casting.

Tailored Microstructures in Hard Magnets

Objective

Improve hard magnets by understanding, in terms of the microstructures achieved, the magnetic and mechanical properties of materials produced by a number of synthesis and processing approaches.

Highlights

- By separating $Nd_2Fe_{14}B$ single domain particles by a non magnetic metallic (Nd) matrix, the largest coercivity ever reported in the ternary Nd-Fe-B system at room temperature (27.5 kOe) has been achieved. This coercivity approaches the theoretical coercivity limit.

- An easy-to-use theoretical model of chemical bonding and thermodynamics of alloys and compounds of rare-earth (RE) and transition (TM) elements has been developed. The model was successfully used to investigate the thermodynamics and defect structures of the Sm-Co system and has great promise for understanding and optimizing processing methods for RE/TM magnets.

- A solidification model that describes the variation in microstructure observed in Nd-Fe-B alloys over a wide range of compositions and quench rates has been developed. The model explains the microstructures of both melt-spun ribbon and inert gas atomized powder and underscores the influence of undercooling, relative to the peritectic temperature, on microstructure.

Processing for Surface Hardness

Objective

Understand the critical synthesis and processing issues which limit the use of plasma-based processing for surface hardness and use this understanding to improve the hardness of thin films and coatings.

Highlights

- A process for the deposition of hard carbon coatings on gears for MEMS applications was developed. These coatings are expected to significantly reduce friction and wear (and possibly stiction) in micromachines and should have numerous other applications.

- A low-temperature sputtering process for the deposition of very hard boron carbide coatings has been developed. Thin films deposited at room temperature on a silicon substrate biased at -25V exhibited a hardness of about 40 GPa, or 20 times that of mild steel. The process opens the door for coating temperature-sensitive materials such as polymers.

- N^+ ion implantation of as-deposited, adherent hexagonal boron nitride films in a certain range of ion energies leads to the formation of cubic bonding and strong enhancement of film hardness without loss of adhesion. Similar implantation of boron increases its hardness to 40 GPa, nearly the value of cubic boron nitride.

Mechanically Reliable Surface Oxides for High-Temperature Corrosion Resistance

Objective

Generate the knowledge required to establish a scientific basis for the design and synthesis of improved (slow growing, adherent, sound) protective oxide coatings and scales on high temperature materials without compromising the requisite bulk material properties.

Highlights

- It has been shown that whereas elimination of sulfur in the underlying FeAlCr alloy can greatly improve the adhesion of alumina scales, the presence of small amounts of reactive elements such as zirconium in the alloy makes the scale-alloy interface even stronger. Thus the role of the reactive elements is more than that of an impurity scavenger.

- Ruby fluorescence and finite element modeling (FEM) are shown to be complementary tools in investigating stress gradients and failure locations in alumina scales that grow during oxidation of FeCrAl alloys. While the ruby fluorescence has been used to measure the hydrostatic stresses, the FEM analysis provides detailed information about all stress and strain components, but it relies on the fluorescence results for validation.

- Positron annihilation spectroscopy has been shown to be effective in characterizing vacancies and vacancy clusters and their distribution in alumina films on Fe and Ni aluminides, examining the influence of dopants on defect structures, and determining changes in substrate defect distributions due to diffusion processes during oxide growth.

High Efficiency Photovoltaics

Objective

Generate advances in scientific understanding that will impact the efficiency, cost and reliability of thin film photovoltaics cells by addressing short-and long-term basic research issues.

Highlights

- Significant progress has been made in understanding the scientific issues that limit the mobilities and carrier lifetimes of the new semiconductor alloy system, GaInNAs. Compositions of this system with bandgaps near 1eV are essential for the development of 4-junction solar cells with predicted conversion efficiencies exceeding 40%.

- An optically-assisted, low-temperature process for enhancing the grain size of thin Si film has been developed. A device structure employing such films has the potential for producing high efficiency (~18%), low-cost solar cells.

- Positron annihilation has provided the first identification of the negatively charged Si dangling bond/Phosphorous complex defect in a-Si:H. The quantitative information about defects from this technique should lead to a better understanding and control of the structure and electronic properties of a-Si:H.

Design and Synthesis of Ultrahigh-Temperature Intermetallics

Objective

Generate the knowledge required to establish a scientific basis for the processing and design of transition-metal silicides with improved metallurgical and mechanical properties at ambient and high temperatures. The ultimate goal is to develop scientific principles to design new-generation materials based on silicides for structural applications at and above 1400°C.

Highlights

- First-principles calculations complemented by neutron diffraction experiments have shown a significant decrease in the thermal expansion anisotropy (which should result in less microcracking during processing) of Mo_5Si_3 by the addition of boron which changes the structure from the $D8_m$(T1) to the $D8_1$(T2) phase. The calculated elastic constants provide insights into the bonding mechanism and form the basis for dislocation modeling.

- Studies of the effects of composition and processing have shown that the addition of boron yields high-temperature strengths of Mo-Si alloys that are superior to that of $MoSi_2$ and results in strengths comparable to those of SiC and Si_3N_4.

- Alloying studies have shown that the addition of 1-10 at.% Al to Mo_5Si_3 retains the T1 phase whereas B addition results in largely the T2 phase which has several extremely desirable high temperature properties, including 30% higher hardness and fracture toughness. In addition, the grain boundary cracking problem is virtually eliminated in the latter phase indicating that the thermal expansion anisoropy of the T2 phase is much less than that of the T1 phase in agreement with Fu et al's theoretical results.

- Stress-strain results and TEM studies of the dislocation structure have shown that the T2 (Mo_5SiB_2) based three-phase alloys have superior high-temperature properties compared to Mo_5Si_3. A fine-grained Mo-9.4Si-13.8B alloy produced by powder metallurgy processing methods exhibited high plasticity above 1400°C as well as high strength of about 140 MPa at a strain rate of $10^{-4}s^{-1}$ - comparable to the strength of some tungsten-based alloys.

Research Briefs

Constitutive Equations for Metal Forming: Texture Considerations

M. G. Stout, U. F. Kocks, S. R. Chen, and C. Tom, Los Alamos National Laboratory,
R. B. Thompson, Ames Laboratory, S. R. MacEwen, Alcan International,
G. Sarma and B. Radhakrishnan, Oak Ridge National Laboratory,
A. J. Beaudoin, University of Illinois

Motivation—Aluminum alloy 5182 has potential applications as an auto body alloy for the production of lighter and, hence, more fuel efficient vehicles. Very large materials changes occur during processing of this alloy, including changes in work hardening, flow stress, mechanical anisotropy, texture, and microstructure. Both a physical understanding of the alloy changes occurring during metal forming and models to simulate the process are required. A wide range of approaches are being combined to accomplish this including: mechanical properties experiments, texture measurements, and microstructural characterization.

Accomplishment—Aluminum alloy 5182 samples were compressed and the constitutive, stress-strain, behavior was measured during the experiments. The different types of stress-strain response are indicative of the operation of different types of deformation mechanisms. At room temperature, 22°C, and slightly above, deformation is characterized by dynamic strain aging. Thermally activated dynamic recovery dominates the deformation mechanism at moderate temperatures while diffusion controlled solute drag governs at high temperatures. The yield stress as a function of strain rate and temperature is described in Fig. 1. Experimental measurements of compression deformation textures are shown as inverse pole figures, to correlate texture with constitutive response and to "unify" the texture development in terms of strain rate and temperature. 5182 develops the classical (101)-fiber compression deformation texture at "low" temperature and "high" strain rates. At "high" temperature and "high" strain rate (001) cube recrystallization texture was observed. At "high" temperatures but "low" strain rates the compression specimens had a bimodal (001) and (101) texture. It is not believed that recrystallization accounts for the (001), (101) bimodal texture, based on these observations. Crystal plasticity theory was used to study formation of the (001) component. Emphasis was placed on identifying the contributions of 1) increased rate sensitivity and 2) slip on the (011) octahedral planes (in addition to slip on the usual 111 octahedral planes). The additional (101) slip system was postulated based on single crystal experiments. Simulations were developed using the LApp (Los Alamos polycrystal plasticity) code, and a discretized representation of the original texture. Results for a simulation with slip admitted solely on the octahedral planes are shown in Fig. 2a. Little evidence of the initial (001) component is noticeable.

Significance—The cube component present in the initial texture is retained during deformation as a result of (011) octahedral slip. This additional slip system is responsible for the bimodal texture observed at "high" temperatures and "low" strain rates. Modeling of texture development during hot rolling, with crystal plasticity theory, must use this non-classical slip system to be accurate. The simulation of recrystallization also includes this slip system.

Contact: M. G. Stout, Los Alamos National Laboratory
Phone: (505) 667-6750, Fax: (505) 665-4013, E-mail: mstout@lanl.gov

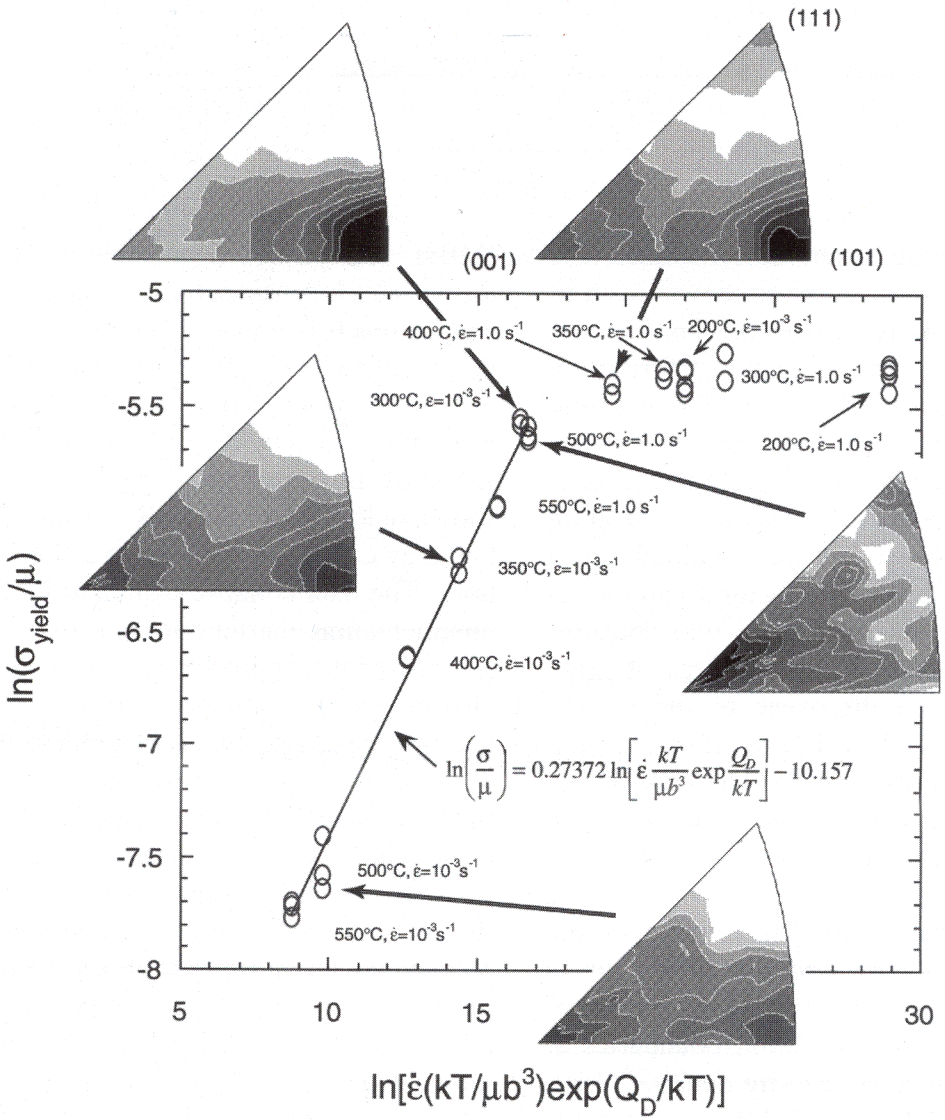

Figure 1. A plot showing the superposition of constitutive behavior and texture development. The (001) cube texture exists for "high" temperatures and both "high" and "low" strain rates.

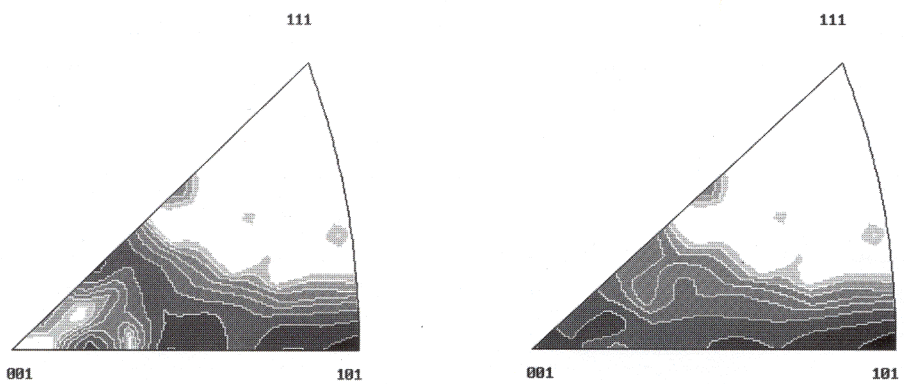

Figure 2. (a) The compression deformation texture calculated assuming only octahedral slip planes. (b) Crystal plasticity calculation based on both (111) and (101) slip planes.

Evolution of Deformation Microstructures

D. A. Hughes and A. Godfrey, Sandia National Laboratories, California,
D. C. Chrzan, Lawrence Berkeley National Laboratory,
Q. Liu and N. Hansen, Risφ National Laboratory, Roskilde, Denmark

Motivation—Large strain deformations take place in many metal forming processes such as sheet forming, forging, extrusion, and rolling. In all these cases, the plastic deformation creates a subdivision of the initial grains into smaller crystallites separated by dislocation boundaries and gives rise to a preferred texture. While the dislocation cell formation and grain refinement have been described qualitatively, a further step is to quantify structural parameters that integrate the microstructure into constitutive laws. Both the common pattern of grain subdivision and the discovery of the scaling relationships described below indicate that general relationships exist which control the evolution of the dislocation structure as a function of the plastic deformation.

Accomplishment—TEM observations of the dislocation structures in a number of fcc metals and alloys reveal a common structural pattern of grain subdivision by dislocation boundaries at two (and sometimes three) size scales. Grain subdivision as a function of different temperatures and alloying content is shown schematically in Fig. 1. In general, two different types of dislocation boundaries are observed: long, continuous dislocation boundaries that have been called geometrically necessary boundaries (GNBs) and smaller scale cell boundaries termed incidental dislocation boundaries (IDBs). The nearly planar GNBs enclose blocks of many approximately equiaxed cells to form a cell block (CB) structure. At small to intermediate strains these GNBs are termed dense dislocation walls (DDWs) and microbands (MBs), depending on whether the boundaries appear singly or in pairs. At each strain level and for each boundary type, an average angle θ_{av}, is calculated from the experimental data and the misorientation data are binned to create histograms. The widely varied probability densities of misorientation angles, $P(\theta,\theta_{av})$ are shown in Fig. 2a for the IDBs. It was discovered that they can all be scaled into a single distribution. The data collapse exhibited by the scaled misorientation distributions is shown in Fig. 2b. An analogous approach can be made for the distributions of boundary spacings. For the boundary spacings, D and D_{av} replace θ and θ_{av}. Remarkably, it is observed that a similar scaling function applies to both the angle and the spacings. The boundary spacings are related to the flow stress. As a further connection between the two parameters, $D_{av}\theta_{av}$ is a constant over the range in which both parameters scale for a given material. While the scaling applies to all of the IDB distributions of Fig. 2b, the scaled GNB misorientation distributions show a somewhat larger data scatter. These deviations may be caused by additional factors controlling the GNB misorientation distribution, especially at larger strains.

Significance—The existence of the scaling relationships for the misorientations and spacings indicates that the deformation structure and its evolution are governed by relatively simple laws for the collective properties of dislocation microstructures produced by plastic deformation. These simple laws can be readily integrated into material constitutive laws.

Contact: Darcy A. Hughes, Sandia National Laboratories, California
Phone: (925) 294-2686, Fax: (925) 844-294-3410, E-mail: darcy_hughes@sandia.gov

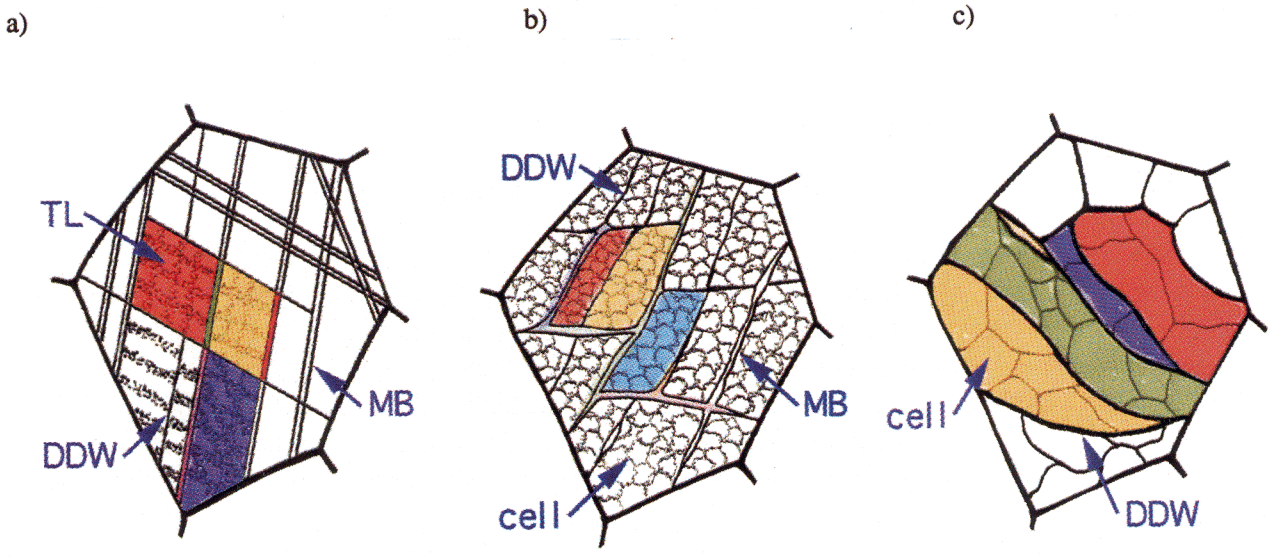

Figure 1. Schematic drawing of deformation microstructures showing grain subdivision occurring in deformed fcc metals and alloys as function of temperature, strain rate, alloy content and stacking fault energy. (a) Grain subdivision in alloys or pure metals with low stacking fault energy or a large friction stress at low to intermediate temperatures; pure metals with medium to high stacking fault energy deformed at extremely low temperatures and high strain-rates. (b) Grain subdivision in pure metals and some alloys with medium to high stacking fault energy deformed at low to intermediate temperatures and alloys deformed at intermediate to high temperatures. (c) Grain subdivision in pure metals and alloys deformed at high temperatures.

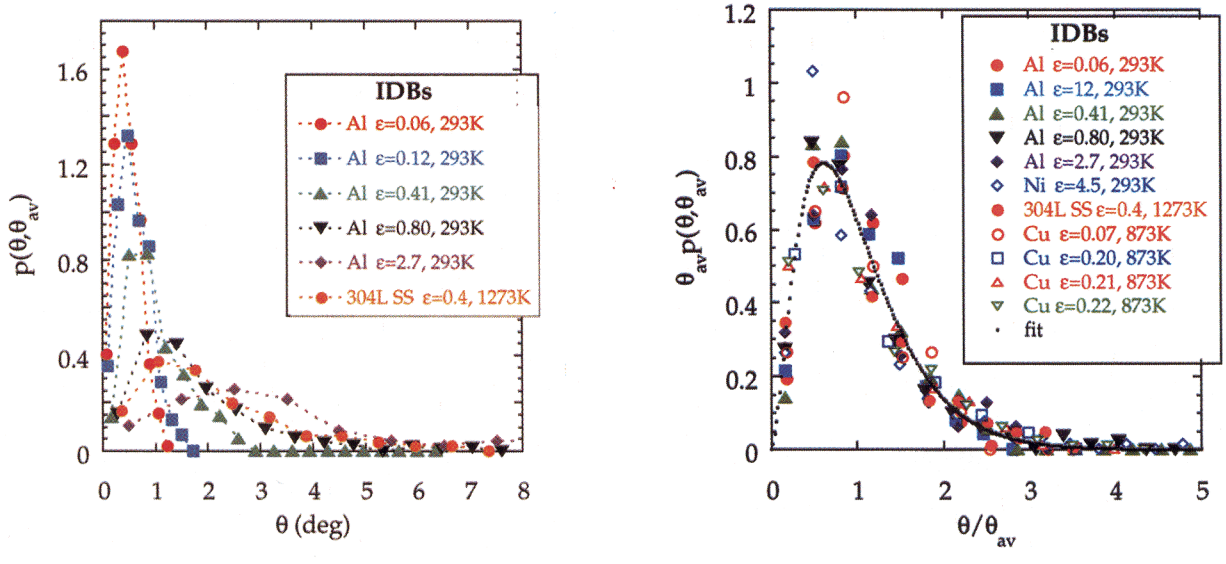

Figure 2. (a) Probability densities of the IDB misorientation angles in different materials deformed under different conditions. (b) Misorientation angle probability densities scale into one distribution using the average angle.

Novel Aluminum Alloy Forming Process

J. S. Vetrano and S. M. Brummer, Pacific Northwest National Laboratory,
L. M. Pawlowski and I. M. Robertson, University. of Illinois,
S. C. Bergsma, Northwest Aluminum Company, Oregon,
T. G. Nieh and J. W. Elmer, Lawrence Livermore National Laboratory,
M. E. Kassner and S. Paddon, Oregon State University

Motivation—Superplasticity and semi-solid forming are processes by which materials can undergo extremely high deformation at high temperatures. Superplasticity generally requires a fine, stable grain size. Often the processing required to achieve fine grains is too expensive for high-volume applications such as in the automotive industry. This research seeks to manipulate the recrystallized grain structure to improve superplastic behavior in a relatively low-cost Al-Mg-Sc based alloy (similar to the commercial alloy 5083) by gaining a better understanding of the role of particles in the recrystallization process. Semi-solid forming traditionally utilizes electromagnetic stirring to produce a fine spheroid size. More economical methods to produce semi-solids with the proper morphology that exclusively utilize thermal treatments are needed.

Accomplishment—Alloys have been heat treated to form two types of Al_3Sc precipitates, coherent and incoherent (Fig. 1). When the precipitates are incoherent, they are typically about 50 nm in diameter (Fig. 1b). Figure 1a shows a dark-field micrograph taken with the superlattice spot from the coherent precipitates and reveals that their size is about 10-20 nm. Their small size and coherency result in a much stronger pinning force on grain boundaries and dislocations.

The tensile elongation as a function of strain rate for the Al-6Mg-0.3Sc alloy is shown in Fig. 2. Micro-structural examination indicates that the presence of Sc in the alloy results in a uniform distribution of fine coherent Al_3Sc precipitates which effectively pin grain and subgrain boundaries during superplastic deformation. The alloy retains fine grain sizes (~7 μm), even after superplastic deformation (>1000%). Dislocations glide across subgrains but are trapped by subgrain boundaries. This process leads to the conversion of pinned low-angle subgrain boundaries to high-angle grain boundaries and the subsequent grain boundary sliding, producing superplasticity.

Semi-solid forming is a method to replace conventional casting processes as less shrinkage, lower temperatures and fewer defects tend to lower costs and give superior properties. Production of semi-solid aluminum alloys such as Al-Si has generally utilized electromagnetic stirring (EM). This work has demonstrated that similar solid-phase morphologies which allow for effective semi-solid forming can be produced less expensively by semi-solid thermal transformations (SSTT), by skipping the EM step. A new, modified, (SSTT) 319 Al-Si-Cu alloy was used for seat belt housing parts in automobiles (Fig. 3).

Significance—By understanding the role of these fine particles in the recrystallization and deformation behavior of the alloy we can have a greater possibility of tailoring alloys for specific mechanical properties. By producing semi-solids exclusively by thermal treatments, novel and inexpensive alternatives to conventional aluminum castings for automotive applications are possible, without a loss of properties.

Contact: John S. Vetrano, Pacific Northwest National Laboratory
Phone: (509) 372-0724, Fax: (509) 376-6308, E-mail: vetrano@pnl.gov

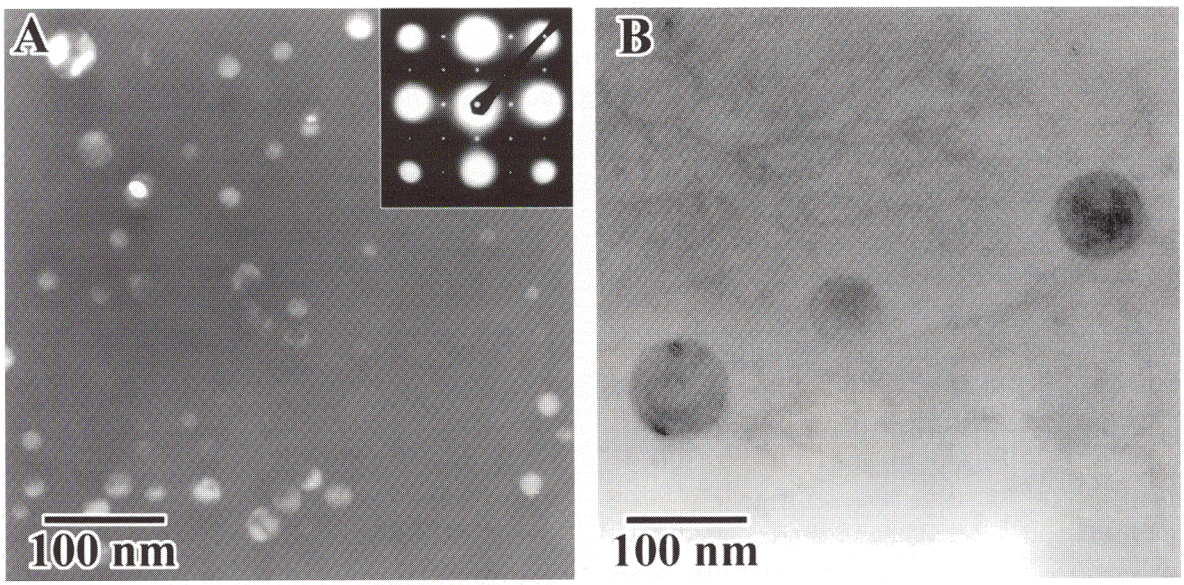

Figure 1. TEM images of Al_3Sc particles following a (a) 300°C/50 hour heat treatment and (b) 500°C/2 hour heat treatment. The dark field image in (a) is taken using one of the superlattice spots shown in the inset diffraction pattern and reveals that the precipitates (bright) are very small and coherent with the matrix. The precipitates in (b) are larger, fewer in number, and incoherent.

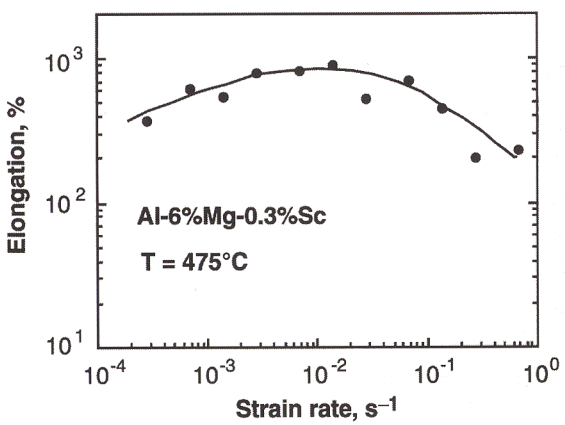

Figure 2. The elongation versus strain-rate of a superplastic Al-Mg-Sc alloy at 475°C.

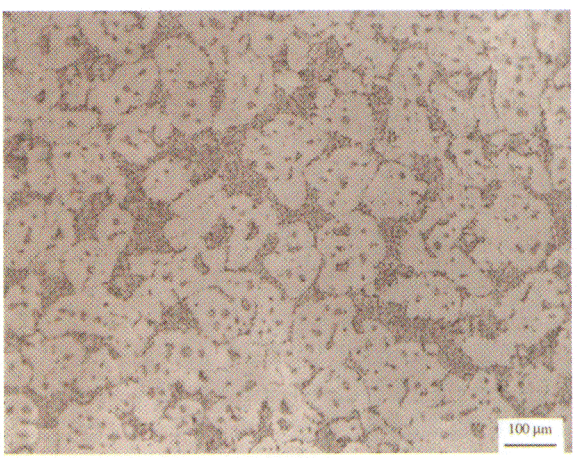

Figure 3. The microstructure of a semi-solid, thermally transformed (SSTT), Al-Si-Cu, modified-319 alloy from an automobile seat belt housing.

High Strength Joints for SiC-Based Systems from Novel Processing Using Solid State Displacement Reactions

C. H. Henager, Jr., C. A. Lewinsohn, PNNL, Richland, WA,
C. Toy and E. Savrun, Sienna Technologies, Inc., Woodinville, WA

Motivation—SiC-based ceramics and ceramic composites are being considered for a variety of applications where joining is an important technology due to the inability to manufacture complex shapes. Ideally, ceramic joints need to be low cost, simple and reliable, high strength, and involve low-temperature and pressureless processing. At this time, it is not possible to address all of these issues with one joining technology and several technologies are being developed. Specifically, it is the scientific basis that links processing, materials chemistry, microstructure, and residual stress to joint strength and reliability that is lacking in the field of dissimilar materials joining and which provides the main motivation behind the varied approaches of the Center's Materials Joining project.

Accomplishment—Solid state displacement reactions, which have been used to produce strong, moderately tough materials, have now been adapted to produce strong joints between SiC-based materials. This has been accomplished through a cooperative effort between Sienna Technologies and PNNL using displacement reactions originally developed at PNNL for the Office of Naval Research. Displacement reactions between Si and Me-C, where Me is a Group IVB, VB, or VIB transition metal like Mo, Nb, or Ti, produce SiC particles in a Me-Si/Me-Si-C matrix. The production of SiC during the reaction makes it thermodynamically favorable for strong bonding to occur at an existing SiC interface. A simple and reliable process, screen-printing technology, has been adapted to making strong joints between SiC materials. Joints are produced by reacting TiC with Si to form $TiSi_2/Ti_3SiC_2$ containing SiC particles (typically elongated particles, Figure 1). The joints are processed at 1350C and 1500C using a small amount of pressure. Joint strengths exceeding 200 MPa in flexure have been achieved at room temperature and strengths approach 350 MPa at 1000C since the Ti_3SiC_2 material undergoes plastic deformation above 900C (Figure 2).

Significance—The ability to produce high-strength joints between SiC-based materials has been demonstrated using technology originally developed to produce in-situ composites. The process has been adapted to use simple application technology, such as screen-printing, but still requires high-temperature processing. Although this represents a drawback for SiC-based composites made with current Nicalon fibers, advanced, stoichiometric SiC-fibers will not have this low-temperature restriction. The major significance is that displacement reaction technology can be transferred to the making of strong joints between materials that possess a chemical similarity to one of the reaction products. For example, reactions that produce alumina can be used to bond alumina-based materials, high-temperature metals such as Mo and Nb can be used, and joints can be tailored and graded as demonstrated in the NiAl-NiO system.

Contact: C. H. Henager, Jr., PNNL
Phone: (509) 376-1442, Fax: (509) 376-0418, E-mail: chuck.henager@pnl.gov

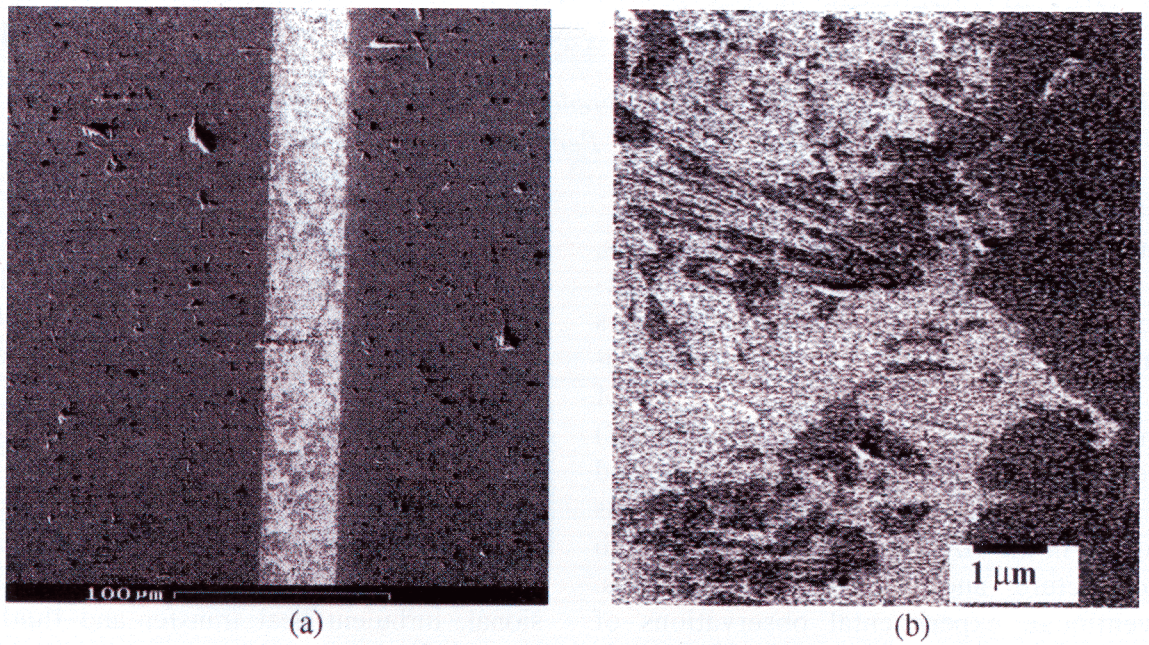

Figure 1. Joint microstructure (SEM) of displacement reaction joint between Hexaloy SiC using screen printing and hot-pressing at 1500C. Joints are thin, strong, and contain homogeneous distributions of SiC particles in Ti_3SiC_2 matrix with some residual $TiSi_2$.

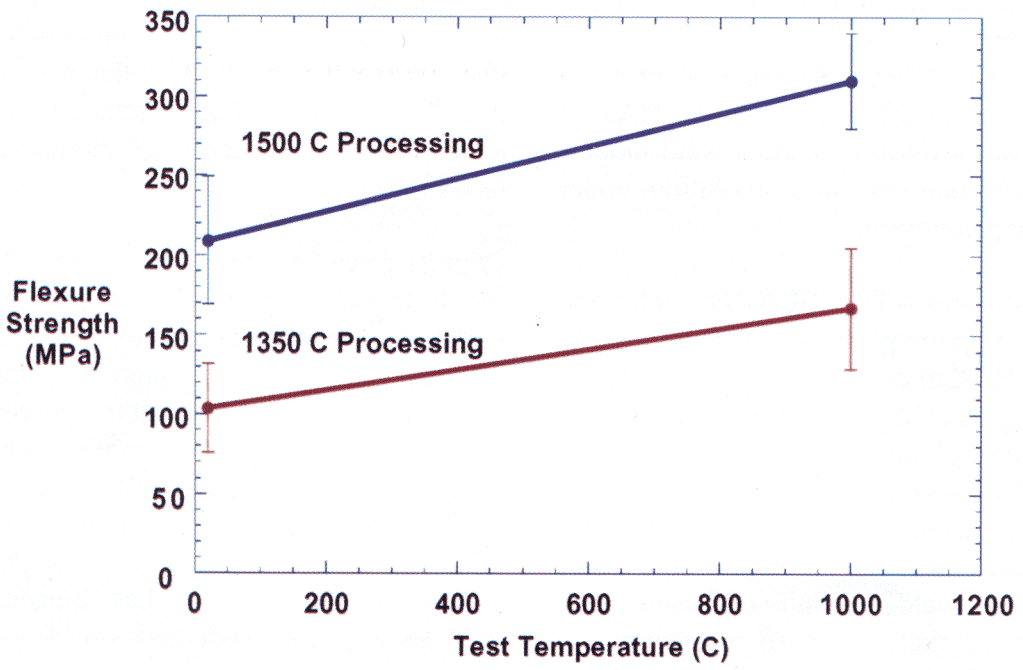

Figure 2. Joint strengths measured in 4-point flexure butt-joint geometry at the indicated test temperature in air. The reaction is more complete and the products are denser after 1500C processing, which influences joint strength. The strength increase with increasing test temperature mirrors previous work in the Ti_3SiC_2/SiC system by the authors.

Real-Time Investigations of Microstructural Evolution in the Heat Affected Zone of Welds Using Spatially Resolved X-ray Diffraction and Numerical Modeling

J. W. Elmer and Joe Wong, Lawrence Livermore National Laboratory,
T. DebRoy and Z. Yang, Pennsylvania State University

Motivation—Severe temperature gradients, high peak temperatures and rapid thermal fluctuations occur as a welding heat source passes through a material. These temperature fluctuations non-uniformly alter the microstructure of the material to create a heat affected zone (HAZ) between the liquid weld pool and the unaffected base metal. Solid state phase transformations that occur in the HAZ create a gradient of both microstructure and mechanical properties. Conventional, experimental observations of HAZ phase transformations are very difficult to obtain because of the extreme thermal conditions and steep thermal gradients that exist during welding. Without experimental verification of these phase transformations, real time models of HAZ microstructural evolution have rarely been attempted and have never before been verified. In this Center work we utilize unique synchrotron-based spatially resolved X-ray diffraction (SRXRD) technique to measure real time phase transformations in the HAZ of welds, and we develop numerical weld models of real time microstructural evolution under actual welding conditions.

Accomplishment—The SRXRD technique was used to map the phase transformations that occur in the HAZ of commercially pure titanium which undergoes an $\alpha \rightarrow \beta \rightarrow \alpha$ phase transformation. Regions of annealing, recrystallization, partial $\alpha \rightarrow \beta$ transformation and complete $\alpha \rightarrow \beta$ transformation were identified. Figure 1 shows a map of these regions with respect to the center of a 1.9 kW arc weld. Results of these experiments indicated that the $\alpha \rightarrow \beta$ transformation was dominated by long range diffusional growth on the leading (heating) side of the weld, while the $\beta \rightarrow \alpha$ transformation was characterized to be predominantly massive on the trailing (cooling) side of the weld with a massive growth rate on the order of 100 μm/s.

The kinetics of phase transformations that occur under the highly non-isothermal heating and cooling cycles produced during welding were studied with the aid of a transient, three-dimensional, turbulent heat transfer and fluid flow model and modified Johnson-Mehl-Avrami formalism. These results successfully predicted the region of $\alpha+\beta$ coexistence around the weld pool, and indicated that the kinetics of the $\alpha \rightarrow \beta$ transformation were controlled by the transport of Ti atoms across the α/β interface. The model further predicted the region where the complete transformation to the β phase had occurred. Real-time evolution of the grain structure in the single-phase β region was modeled using a three dimensional Monte Carlo technique developed to account for the steep HAZ thermal gradients (see Fig. 2).

Significance—Understanding the kinetics of phase transformations that occur under the highly non-isothermal and extreme conditions of welding is the key to predicting the effects that weld parameters have on the microstructure and integrity of welded joints. Through a combination of in-situ SRXRD-based experiments and numerical modeling of real time microstructural evolution, it is now possible to study the kinetics of HAZ phase transformations in welds with unprecedented confidence.

Contact: J. W. Elmer, Lawrence Livermore National Laboratory
Phone: (925) 422-6543, Fax: (925) 423-7040, E-mail: elmer1@llnl.gov

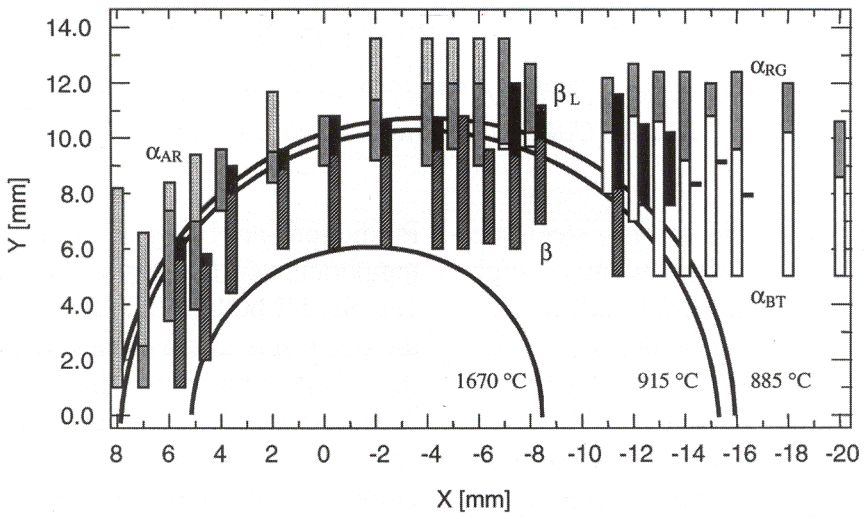

Figure 1. SRXRD map comparing the experimentally determined locations of the diffraction patterns with the calculated weld isotherms. The weld is moving from right to left and symmetry is assumed about the weld direction. Locations of the α_{AR}, α_{RG}, α_{BT}, β and β_L diffraction patterns are indicated. The notations are: AR = annealed and recrystallized; RG = recrystallized undergoing grain growth; BT= back-transformed; β = high temperature bcc; and L = low amount of β present. Details are provided in: J. W. Elmer, Joe Wong and Thorsten Ressler, *Metall. Mater. Trans. A*, 1998, vol. 29A(11), p. 2761.

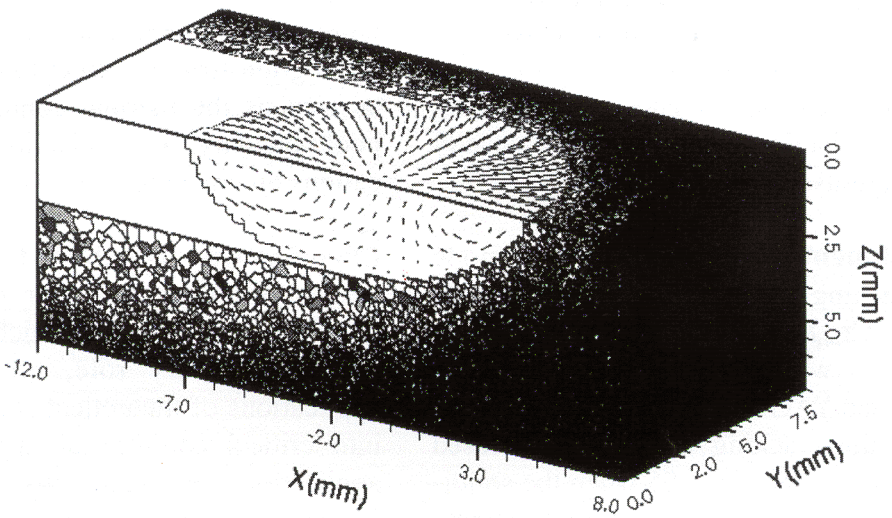

Figure 2. Monte Carlo calculations of real time grain structure distribution around the weld pool in three dimensions using 400x200x150 grids. The calculated liquid weld pool is moving left to right, and the arrows indicate the fluid flow vectors. Details are provided in: Z. Yang, J. W. Elmer, Joe Wong and T. DebRoy, submitted to the *Welding Journal.*

Solidification Behavior and Cracking Response of Laser Welds in Austenitic Stainless Steels

J. Brooks and C. Robino, Sandia National Laboratories,
S. David, Oak Ridge National Laboratories

Motivation—The austenitic stainless steels are used in the manufacturing of many small, high quality components made from sulfur (S)-containing alloys. High energy density (HED) welding processes that produce very small, low heat input welds are often required. However, major problems exist in that the solidification mode of the rapidly solidified HED welds can be different from those of more conventional processes. This can drastically increase cracking susceptibility that is further aggravated by high levels of S promoting the formation of low melting liquids. The solidification mode of conventional welds can be related to the Cr_{eq}/Ni_{eq} ratio, and alloys that solidify as ferrite are much more resistant to cracking than those solidifying as austenite. The change in solidification mode occurs at a ratio considerably higher for HED than conventional welds, and the ratio is not a good predictor at high solidification rates over wide ranges of compositions. In this work we are establishing weld cracking behavior of S containing stainless steels and are predicting solidification behavior from thermodynamically based calculations.

Accomplishment—The solidification mode and weld cracking behavior of a series of alloys of different Cr_{eq}/Ni_{eq} ratios and S contents (0.4wt% max.) were evaluated with both the GTA and pulsed YAG welding processes. In the GTA welds the cracking resistance increased drastically for $Cr_{eq}/Ni_{eq} > 1.55$ when the solidification mode changed from austenite to ferrite. However due to the shift in solidification mode Cr_{eq}/Ni_{eq} ratios of ~1.75 or greater were required to prevent cracking of the YAG laser welds at the higher levels of S in the limited range of compositions studied.

Predictions are being made of the solidification temperature of the dendrite tip as a function of velocity for both the ferrite and austenite phases, the one stable at the highest temperature will be the first phase to form, see figure 2. Thermodynamic programs are being used to calculate the partitioning coefficients for each alloying element that is needed in calculating dendrite tip temperature. However these calculations are complicated by the many alloying elements contained in commercial alloys: Cr, Ni, Mn, Si, N, C and S. It was further found using Backscattering Electron Kikushi Patterns (BEKP), that in pulsed YAG welds with a Creq/Nieq ratio of ~1.75, some grains solidified as ferrite and massively transformed to austenite while others solidified completely as austenite. This mixed solidification mode behavior is attributed to growth along preferred crystallographic directions. Dendrite tip velocities are dependent upon orientation of the individual HAZ grain from which epitaxial growth occurs as well as the thermal conditions at the weld pool boundary. This behavior has further implications on cracking behavior.

Significance—The ability to accurately predict the solidification behavior of these complex commercial alloys in which phase selection plays a primary role, greatly extends the applications of theoretical solidification models into critical commercial applications. These applications are numerous. As shown here certain compositions of stainless steel alloys with high levels of sulfur are weldable with the pulsed YAG process if the solidification mode occurs as ferrite. Predictions of solidification behavior for different processing conditions and compositions are thus extremely important.

Contact: J. A. Brooks, Sandia National Laboratories
Phone: (925) 294-2051, Fax: (925) 294-3410, E-mail: jabrook@sandia.gov

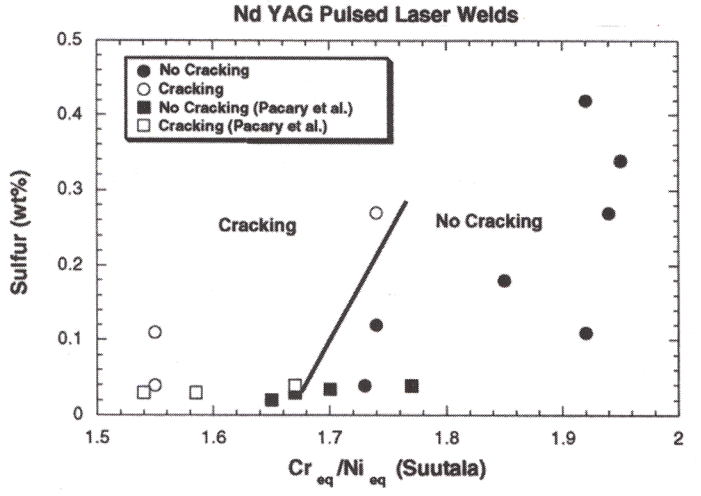

Figure 1. Cracking response of Pulsed YAG laser welds showing that welds solidifying as primary ferrite (in the no cracking region) are very resistant to weld cracking even at high levels of sulfur.

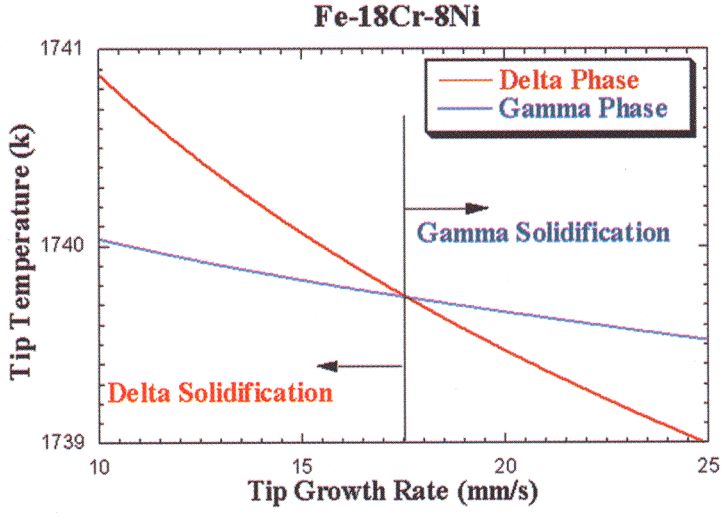

Figure 2. Calculations of solidification mode as a function of velocity for both ferrite and austenite phases using the KGT model. The solidification mode changes from ferrite to austenite at velocities above 17mm/s.

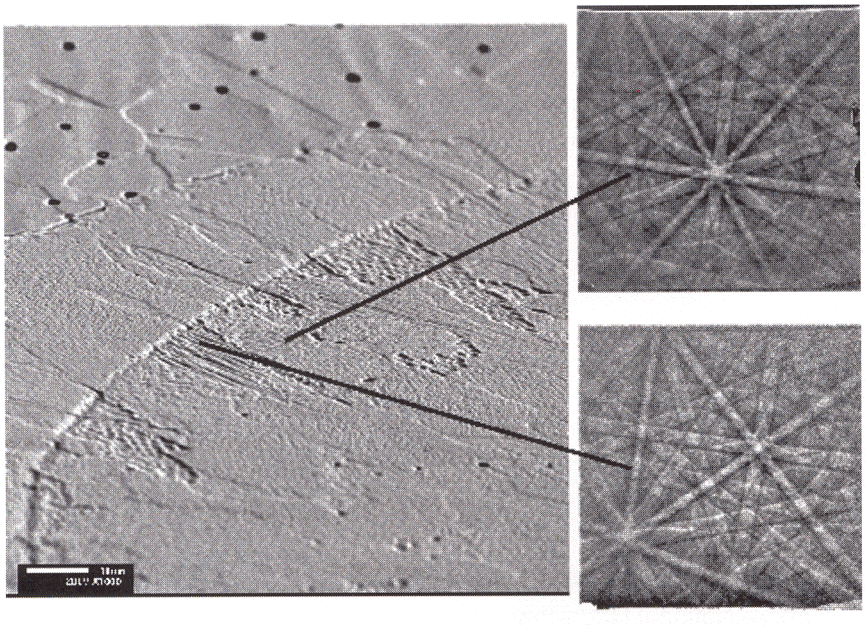

Figure 3. Pulsed YAG laser weld showing two adjacent grains one that solidified as ferrite and the other as austenite, BEKP shows that as a result of a ferrite to austenite massive transformation both grains are single phase austenite at room temperature.

Processing-Derived Porosity in Carbon Aerogels

T. D. Tran and *L. W. Hrubesh*, *Lawrence Livermore National Laboratory,*
K. Kinoshita, *Lawrence Berkeley National Laboratory,*
M. S. Dresselhaus, *Massachusetts Institute of Technology* and *M. Droege*, *Ocellus, Inc.*

Motivation—The unique morphology of aerogels with exceedingly high surface areas is manifested by a nanometer-sized interconnected network of pores in the supporting matrix particles which then arrange to form a mesoporous architecture. Attendant properties of these organically-derived substances are markedly influenced by microporosity on both of these length scales in analogy to oxide-based inorganic materials. Carbon aerogels have many uses, which depend upon enhanced transport of electrons, ions, and molecules through the materials. These materials have recently found applications in electrochemical power storage cells (supercapacitors) as well as in electrosorptive deionization cells for desalinizing water. While desirable properties have been achieved, the full potential of these materials has not been realized. Ongoing research in this Center project strives to establish inter-relationships between processing, structure, and properties with a goal of improving aerogel performance and reliability.

Accomplishment—The most common carbon aerogels, derived from organic precursors made by the aqueous polycondensation of resorcinol (1,3 dihydroxybenzene) and formaldehyde can be produced as monoliths, thin films, or microspheres as seen in Figure 1. While monolithic RF carbon aerogels exhibit the most ideal properties and have been widely studied, thin carbon aerogel composites, containing a commercial carbon paper on which carbon aerogels have been deposited, are more widely used in many electrochemical applications. These electrode composites possess characteristics close to those of monolithic materials, and they have been prepared inexpensively, without the need for supercritical solvent extraction. Our recent work has demonstrated that processing conditions can have a significant effect on attendant aerogel properties. The Table, which accompanies Figure 1, shows how material properties vary with the initial batch composition (resorcinol-formaldehyde ratio). Pyrolysis temperature also was found to influence aerogel properties. Based upon these studies, optimum processing conditions have been found for producing a material with tailorable pore morphology and targeted properties.

Significance—New polymeric aerogel compositions can be achieved using simple drying protocols which do not require time consuming, costly, solvent exchanges and supercritical fluid solvent drying. Carbon aerogels with larger pore sizes and higher surface areas can be prepared from gels by simple thermal modifications. Such materials provide increased performance in supercapacitor and desalinization applications.

Contact: L. W. Hrubesh, Lawrence Livermore National laboratory
Phone: (925) 423-1691, Fax: (925) 423-4897, E-mail: hrubesh1@llnl.gov

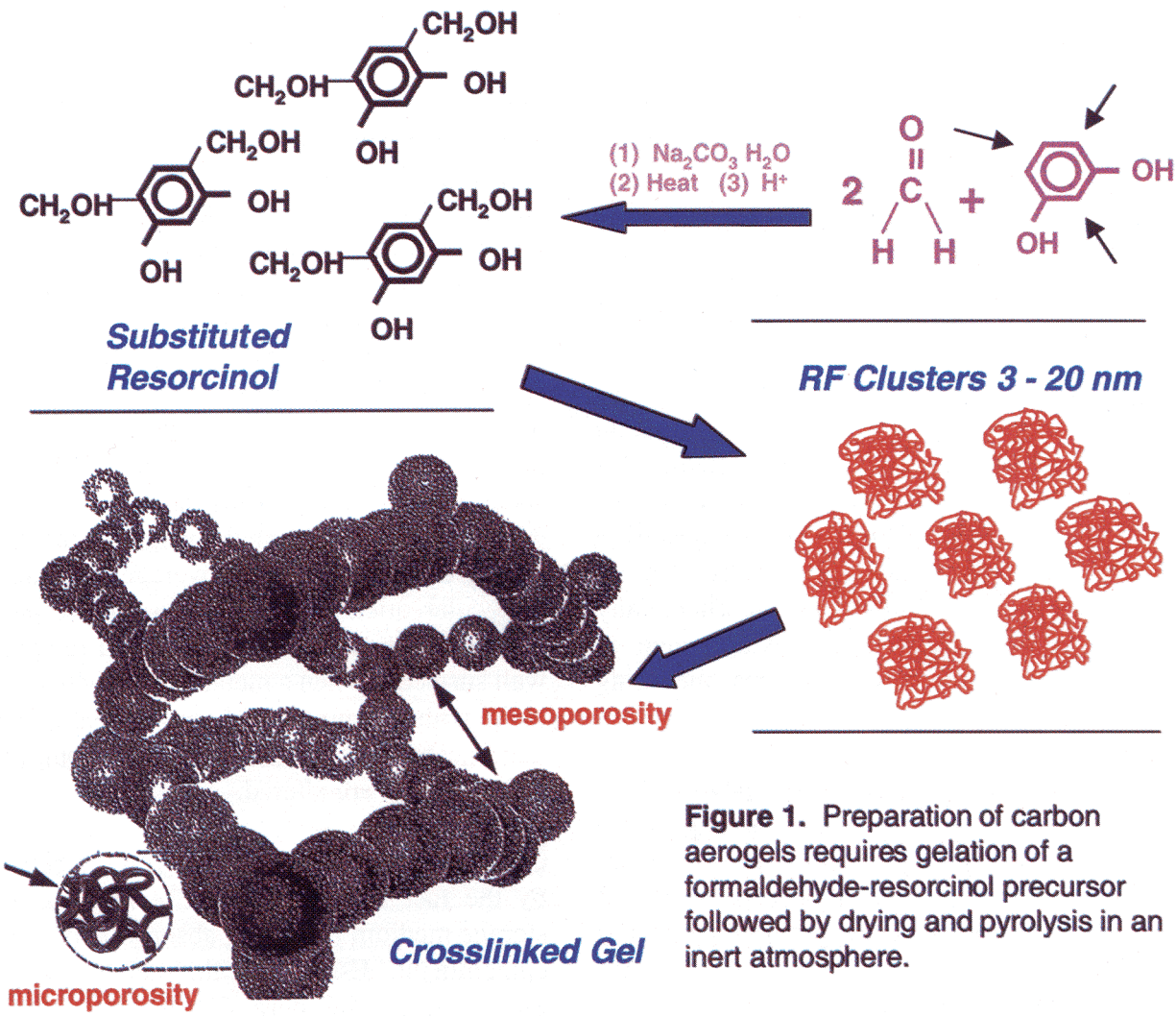

Figure 1. Preparation of carbon aerogels requires gelation of a formaldehyde-resorcinol precursor followed by drying and pyrolysis in an inert atmosphere.

Carbon Aerogel Properties

Aerogel	wt % R/F	ρ (gm/cc)	S.A. (m^2/g)	Pore Size (A)	Capacitance (F/g)
monolithic	40	0.58	666	65	34
monolithic	50	0.83	580	50	28
composite	70	0.6	360	80	17
composite	50	0.41	389	170	17.8
composite	60	0.47	408	56	19.0
composite	70	0.60	297	37	0.9
composite	60	0.40	623	77	14.9
composite	60	0.43			23.0
composite	60	0.43	589	77	28.4
composite	60	0.45			
composite	60	0.44	399	61	17.8

Molecularly-Tailored Ceramic Composites

Jun Liu, G. E. Fryxell, and L. Q. Wang, Pacific Northwest National Laboratory

Motivation—As part of a coordinated effort in this Center project to develop nanocomposites with tailorable properties, ceramic materials with ordered pore architectures have been infused with molecules of a specific size and chemical functionally to form dense monolayers on the wall surfaces within the nanometer porosity. Self-Assembled Monolayers on Mesoporous Supports SAMMS integrates the mesoporous ceramics technology first developed by Mobil Oil Corporation with an innovative method for attaching chemically specific molecules to the oxide surface. In addition to sequestering mercury, lead, chromium, and a cadre of other metal cations, the SAMMS can be chemically tailored to selectively bind a wide range of mixed waste contaminant species including radionuclides.

Accomplishment—SAMMS is produced in bead or powder form. Each grain of material, in this case a type of silicate, is ~10 μm in diameter and contains a dense ordered array of cylindrical caverns or pores, giving the material a honeycomb appearance (Fig. 1) with concomitant large surface area. Resident pores function as templates where the chemically tailored monolayers reside. The molecules, which comprise these pore surface layers, bind strongly at one end to the ceramic support material. The free end of the tethered molecule is then available for complexation with a targeted metal species passing through the pore. Upon release in water or other liquid, SAMMS quickly immobilizes a targeted metal species thereby reducing the metal ion concentration far below drinking water standards. (Fig. 2) The small pore size also precludes egress of bacteria, which could resolubilize the metal into a more toxic and/or mobile form. The key to the synthesis and properties of these encapsulants is associated with the functionalized monolayer and its interaction with the ceramic substrate and the targeted cation. Such interactions have been probed by means of ^{13}C magnetic resonance spectroscopy. Fig. 3 illustrates concentration-dependent conformational changes of the bound molecules. At increased coverage, the random molecular orientation orders to a close-packed configuration which is perpendicular to the pore wall surface. When a metal cation such as Hg^{+2} binds with the molecule, both the peak position and lineshape of the terminal head-group in the ^{13}C spectrum are altered.

Significance—SAMMS versatility is reflected by the fact that it also can serve as a waste storage medium following absorption of a metal contaminant. Essentially, the metal is encapsulated within the ceramic material. When subjected to regulatory benchmark tests which measure release under environmental conditions, the bound metal cations were found to be immobilized in the solid and to exhibit markedly low leach rates. SAMMS can be used in water, non-aqueous solutions or gas phase waste streams making the technology potentially amenable to industrial scale recovery and processing operations.

Contact: Jun Liu, Pacific Northwest National Laboratory
Phone: (509) 375-2616, Fax: (509) 375-2186, E-mail: jun.liu@pnl.gov

Figure 1. Schematic drawing of a functionalized mesoporous composite material showing the ordered molecular interface at the pore wall surface.

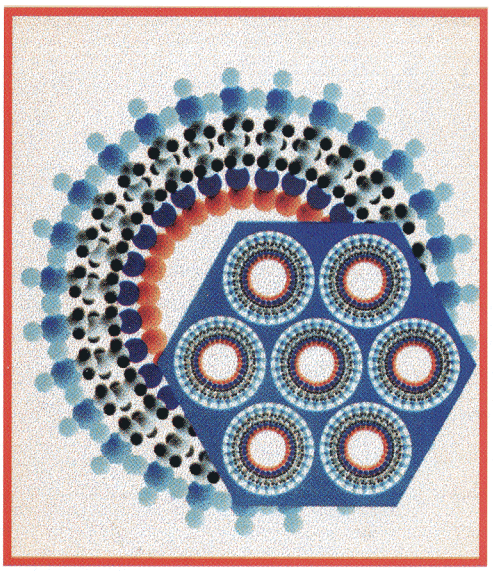

Figure 2. Comparison of Hg^{+2} uptake kinetics and solution equilibrium concentrations for a commercial material (blue curves) and the hybrid mesoporous composite material (purple curves). (a) Initial Hg^{+2} concentration = 50 ppb. (b) Initial Hg^{+2} concentrations = 10 ppm.

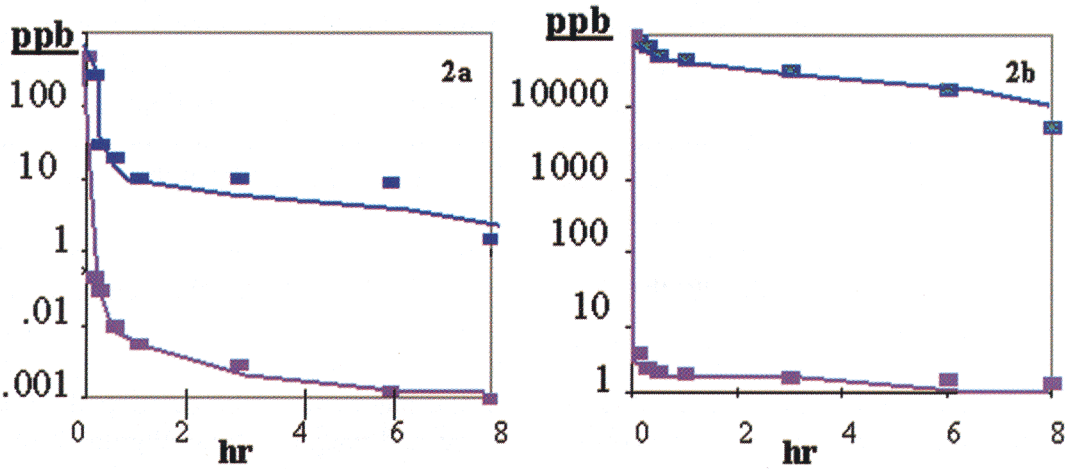

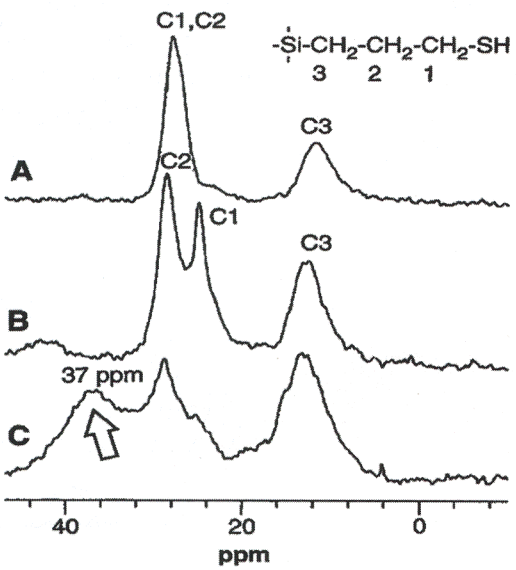

Figure 3. ^{13}C NMR spectra of organic monolayers on mesoporous silica. (A) At 25% coverage, C_1 and C_2 can not be deconvoluted because of conformational heterogeneity. (B) At 76% coverage, C_1 and C_2 are resolved. (C) Upon complexation with Hg^{+2}, a new feature is observed at 37 ppm..

Polymer Derived Nanocomposites with Tailored Properties

D. L. Gin, University of California, Berkeley, LBNL,
J. A. Reimer, University of California, Berkeley, LBNL

Motivation—A novel class of functional, nanostructured polymeric materials has been developed through polymerization of amphiphilic liquid crystal (LC) assemblies. By incorporating a secondary phase within the organized nanochannels, unusual materials properties have been realized. Such nanoporous polymers are capable of catalyzing organic reactions because of the high local concentration of ionic head groups lining the channels. The unique environment inside these nanochannels is likely responsible for the unusual physical and chemical properties observed. Ongoing coordinated research in this Center project concerns the use of solid-state NMR spectroscopy to investigate the environment inside the nanochannels. A second motivation is to use magnetic fields and other resources to macroscopically align the LC assemblies prior to cross-linking, in order to optimize the bulk properties of these systems.

Accomplishment—Solid-state ^{23}Na NMR is used to probe the interior of these nanostructured polymeric materials. In Figure 1, the ionic sodium carboxylate headgroups of the LC monomers aggregate to define the aqueous nanochannels. The T_1 relaxation times of ^{23}Na confined in the nanochannels, which provide valuable information on the mobility of ^{23}Na and the symmetry around the ions, are compared with those of several sodium standards in Table 1. The very short T_1 time is likely due to the high mobility of Na^+ ions along the channel walls. Results suggest that carboxylates lining the channel may form an ordered arrangement, which promotes ion mobility in the solid. Shearing of the inverted hexagonal LC assembly prior to polymerization induces orientation such that the nanochannels lie on average parallel to a substrate surface. Experiments suggest that alignment of the channels perpendicular to a film surface can be achieved by thermally annealing the inverted hexagonal phase in a 9.4 T magnet prior to polymerization. (Fig. 2) The degree of bulk alignment in the magnetically aligned system is not as high as that of a shear-aligned sample, but some degree of alignment has been confirmed from the data.

Significance—By using solid-state NMR techniques, the local chemical environment inside ordered nanotubes can be characterized. Results will enable protocols for structural manipulation at the nanoscale to be developed. Preliminary shear and magnetic field alignment results have demonstrated that conventional processing techniques can be applied to the hexagonal LC assemblies for extending the intrinsic small-scale order to the macroscopic scale. This opens up the possibility of integrating processing with chemical control to optimize the properties of these new materials.

Contact: Doug Gin, University of California, Berkeley
Phone: (510) 642-7756, Fax: (510) 643-1846, E-mail: gin@cchem.berkeley.edu

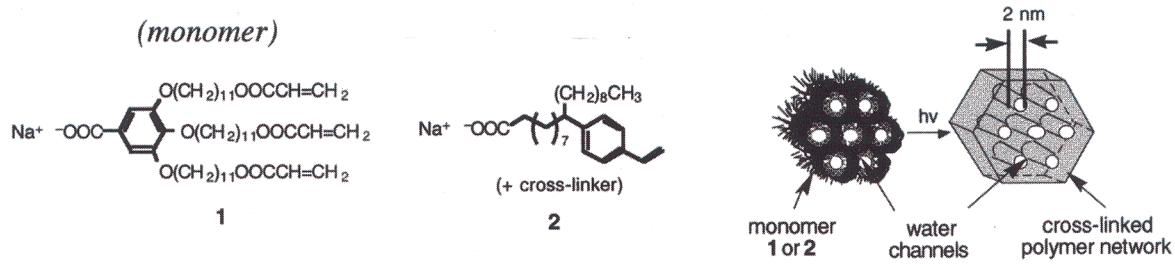

Figure 1. Formation of nanoporous, nanostructured polymers via photo-crosslinking of the inverted hexagonal LC phase.

Sample	T_1 (ms)
Sodium Chloride	1×10^4
Sodium Benzoate	2×10^3
Polyacrylic Acid, Sodium Salt	1
Cross-linked LC Phase of Fig. 1	2

Table 1. ^{23}Na T_1 relaxation times measured using inversion recovery on a 400 MHz magnet.

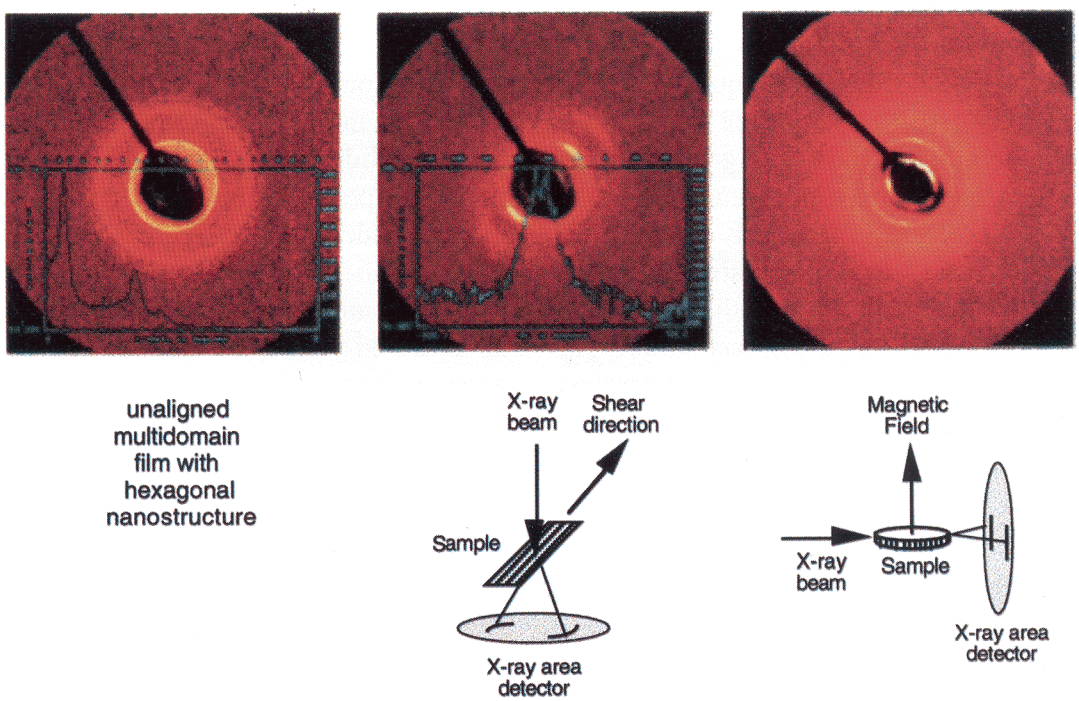

Figure 2. 2-D X-ray diffraction profiles of an unoriented sample, a shear-aligned sample, and magnetic field aligned sample of the inverted hexagonal LC phase of the Co(II) salt of the monomer. All samples were crosslinked following orientation.

Comprehensive Model for a Rapidly Solidified Peritectic System: $Nd_2Fe_{14}B$ A Case Study

R. W. McCallum and M. J. Kramer, Ames Laboratory,
D. J. Branagan, Idaho National Engineering and Environmental Laboratory,
L. H. Lewis, Brookhaven National Laboratory

Motivation—The objective of this work in the Center's Hard Magnets project is to understand the solidification process in Rare Earth permanent magnets in order to optimize the hard magnetic properties as well as elucidate basic structure-property relationships. Both composition and solidification rate are crucial parameters.

Accomplishment—A solidification model that describes the variation in microstructures observed in Nd-Fe-B alloys over a wide range of compositions and quench rates has been developed. The key factors in controlling the microstructural evolution have been identified. The key aspects to this model are shown in the accompanying Figure and are fully consistent with TEM observations. If the initial undercooling does not fall below the glass formation temperature, the primary solidification product is dendrites of 2-14-1. As these dendrites grow into the ribbon away from the Cu quench wheel, the heat produced by recalescence results in a rise in temperature behind the growth front. Under certain condition, recalescence can raise the temperature to the peritectic temperature where 2-14-1 is no longer the stable phase. In the unsolidified region above the peritectic temperature, Fe becomes the primary solidifying phase while the solidified region undergoes grain refinement. Since there is epitaxy between Fe and 2-14-1, the wheel side forms a coarse-grained, but textured 2-14-1 microstructure with filamentary Fe inclusions. This knowledge has enabled the fabrication of melt-spun ribbons with microstructures ranging from amorphous, uniformly nanophased and highly aligned, depending upon slight changes in composition and processing conditions.

This research has shown that the wide variations in the microstructure of rapidly-solidified 2-14-1 ribbons, from nanophased to large c-axis aligned grains, is controlled by the level of undercooling and recalescence relative to the peritectic temperature. When this model is applied to the Nd-Fe-B system it explains the microstructures observed in both the melt-spun ribbon and inert gas atomized (IGA) powder.

Significance—Solidification in peritectic systems is not well understood. Unraveling the nuances of a complex ternary alloy peritectic solidification over a wide range of processing conditions marks a large step in the understanding of solidification in many technologically important peritectic alloy systems. It is shown that the wide variations in the microstructure of rapidly-solidified $Nd_2Fe_{14}B$ (2-14-1), from isotropic nanoscaled to anisotropic aligned microscaled grains, is controlled by the level of undercooling and recalescence relative to the peritectic temperature.

Contact: Matthew J. Kramer, Ames Laboratory
Phone: (515) 294-0276, Fax: (515) 294-4291, E-mail: mjkramer@ameslab.gov

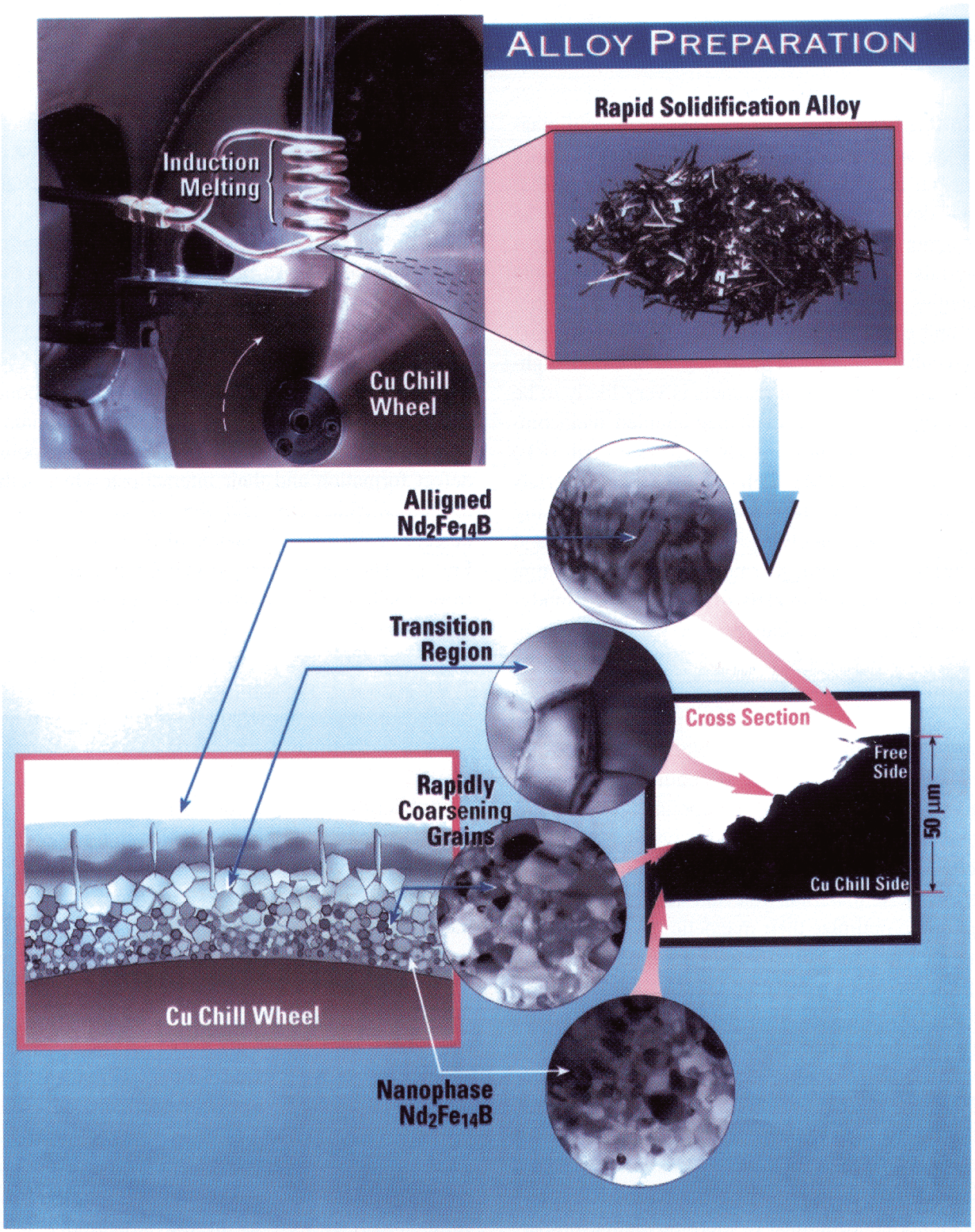
ALLOY PREPARATION
Rapid Solidification Alloy
Induction Melting
Cu Chill Wheel
Alligned $Nd_2Fe_{14}B$
Transition Region
Rapidly Coarsening Grains
Cu Chill Wheel
Nanophase $Nd_2Fe_{14}B$
Cross Section
Free Side
Cu Chill Side
50 µm

Theory of Lattice Defects and Thermodynamics in Rare Earth-Transition Metal Magnets

David O. Welch, Brookhaven National Laboratory

Motivation—High-performance permanent magnets are an essential ingredient of improved, more compact, and more efficient electric motors, electronic devices and sensors. Improvements in the production and performance of permanent magnet materials is an important aspect of technological strategies for increased efficiency in energy production and energy systems and concomitant reduction of greenhouse gases. The next generation of high-performance permanent magnets is very likely to be based on multi-phase exchange-coupled nanocomposites of compounds and alloys of rare-earth (RE) and transition (TM) elements. Such materials require complex and sophisticated processing methods, often involving metastable phases and conditions far from thermodynamic equilibrium. Suitable theoretical models of structure, thermodynamics, and kinetics can play a valuable role in development of such processes which are being pursued in this Center Project.

Accomplishment—A flexible and easy-to-use theoretical model of chemical bonding and thermodynamics in alloys and compounds of RE/TM elements has been developed for understanding the microstructural, thermodynamic, and kinetic properties of these materials relevant to the processing required to optimize their magnetic properties. This semi-empirical model is based on a modern version of Linus Pauling's resonating valence bond theory of metallic bonding, called bond-order potentials, developed by Pettifor and Cottrell. The present work developed a version of bond-order potentials for RE/TM compounds, which incorporates the accurate and widely-used Miedema theory of heats of formation of alloys and compounds, and utilizes a Debye-Grüneisen approach to estimate thermal and vibrational contributions to thermodynamic properties. This model was combined with the statistical thermodynamics of regular solutions to analyze the thermodynamics of point defects, non-stoichiometry, and solute additions in Sm-Co magnet materials. There has been much recent interest in the possibility of producing high-performance exchange-spring nanocomposites based on these materials and other RE/TM compounds. These magnets are processed to form coherent cellular microstructures based on complex processing of the $SmCo_5$-Sm_2Co_{17} region of the phase diagram, shown in Fig. 1. The bond-order potential-based statistical thermodynamic theory was used to derive the energetics of point-defect formation and their interactions which leads to non-stoichiometry and the formation of point defects in the basic structure of $SmCo_5$, shown in Fig. 2. The theory showed that Co-rich deviations from stoichiometry are most easily formed by inserting dumbbell-shaped Co-Co pairs in place of Sm atoms, in agreement with experience (see Fig. 3). The Co-Co dumbbells interact via elastic distortions of the lattice and consequently order their arrangement to form Sm_2Co_{17}.

Significance—The theory permits description of the non-stoichiometric ranges of the two compounds and the two-phase region of the phase diagram, as well as computation of the thermodynamics of metastable phases. The calculations also revealed a propensity for Co atoms to segregate to surfaces and interfaces of $SmCo_5$, a result that has significant implication for the coercivity of these materials (see next Brief by Gert et al). The theory is simple enough to use for complex situations, which often preclude the use of first-principles calculations, yet it contains much of the essential physics. It shows great promise as an aid to understanding processing methods and the effects of solute additions in Sm-Co compounds, as well as in the structurally more complex Nd-Fe-B system.

Contact: D. O. Welch, Brookhaven National Laboratory
Phone: (516) 344-3517, Fax: (516) 344-4071, E-mail: dwelch@bnl.gov

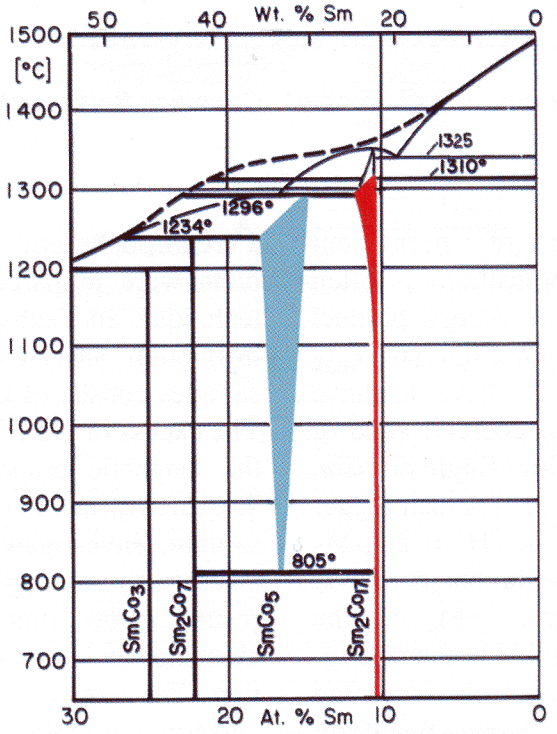

Figure 1. The thermodynamic phase diagram (compiled by K. Strnat) of the Sm-Co system. The region of interest for two-phase nanocomposites is between the blue ($SmCo_5$) and red (Sm_2Sm_{17}) regions of the diagram.

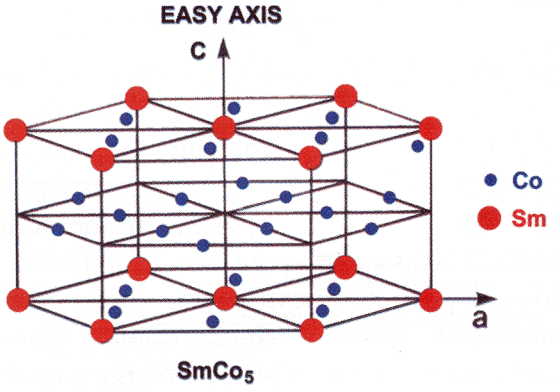

Figure 2. The crystal structure of $SmCo_5$ Replacement of one-third of the Sm atoms by dumbell-shaped pairs of Co atoms produces the Sm_2Co_{17} structure.

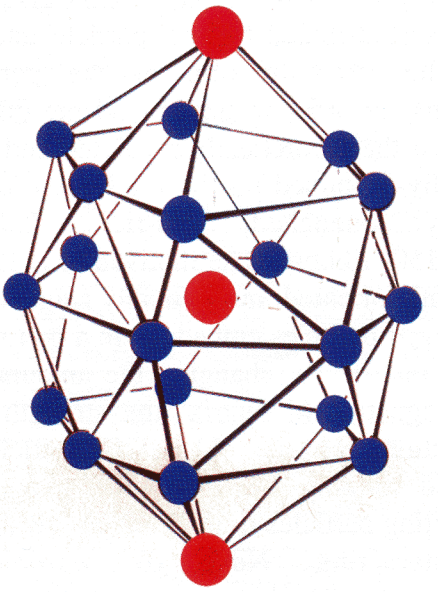

Figure 3. The nearest neighbors to a central Sm atom in $SmCo_5$. It is energetically favorable to make Co-rich $SmCo_5$ by removing the central atom and replacing it by a vertical dumbbell-shaped pair of Co atoms.

Microstructurally Tailored Nd-Fe-B Magnets Approaching Theoretical Coercivity Limits

Er. Girt, K. M. Krishnan, and G. Thomas, Lawrence Berkeley National Laboratory

Motivation—Performance of permanent magnets for a variety of applications is often determined by the maximum energy product $(BH)_{max}$. In order to obtain high $(BH)_{max}$ permanent magnetic materials have to have large coercivity. In theory, the coercive field of ideally oriented, non-interacting, single domain, magnetic particles, assuming K_1 is much bigger than K_2, has been shown to be $H_c = 2K_1/Ms - N M_s$, where K_1 and K_2 are the magnetocrystalline anisotropy constants, M_s is the spontaneous magnetization and N is the demagnetization factor. For randomly oriented non-interacting particles, the Stoner-Wohlfarth model predicts that the value of H_c decreases to about half. However, experimentally obtained values of the coercive fields in permanent magnets are smaller by a factor of 3 to 10 for well oriented samples and by a factor of 2 for randomly oriented samples. This discrepancy has been attributed to inter-particle interaction and the microstructure of the permanent magnets. In order to understand the difference between the theoretically-predicted and experimentally- obtained results for H_c, we prepared rapidly quenched, Nd-rich, $Nd_xFe_{14}B$ ($2<x<150$) ribbons. The motivation is to obtain randomly oriented, magnetically single domain, $Nd_2Fe_{14}B$ particles embedded in a non-magnetic Nd matrix. By changing the amount of the non-magnetic Nd matrix, the strength of the interaction between $Nd_2Fe_{14}B$ particles was tailored ranging from strongly magnetically interacting particles in pure $Nd_2Fe_{14}B$ to nearly non-interacting $Nd_2Fe_{14}B$ particles in $Nd_{150}Fe_{14}B$. The latter is expected to approach the high coercive field predicted by the Stoner-Wohlfarth model.

Accomplishment—$Nd_xFe_{14}B$ ($2<x<150$) ribbons were prepared using the melt spinning technique and subsequently annealed. X-ray diffraction analyses shows that the annealed samples consist of α-Nd, γ-Nd, and $Nd_2Fe_{14}B$. The excess of Nd affects the microstructure and the magnetic properties of Nd-Fe-B ribbons. The microstructure of the annealed $Nd_{40.5}Fe_{14}B$ sample, investigated using AEM (analytical electron microscopy), is presented in Fig. 1. The results show that $Nd_2Fe_{14}B$ particles are elongated in shape with a narrow size distribution. The matrix consists of α-Nd and γ-Nd. Quantitative analysis of the Fe/Nd ratio by EDX (energy dispersive X-ray microanalysis) show that the ratio between Fe and Nd, across the particles, is 83 / 17 consistent with the composition of $Nd_2Fe_{14}B$. The matrix almost entirely consists of Nd with a few percent of Fe also present. The dependence of coercivity in $Nd_xFe_{14}B$ as a function of the Nd-matrix concentration at room temperature is presented in Fig. 2. This is about 80% of the ideal value of coercivity obtained from the Stoner-Wohlfarth model.

Significance—The coercivity can be enhanced more than two times by fully separating the $Nd_2Fe_{14}B$ single domain particle. Using this approach, we have achieved the largest coercivity, 27.5 kOe, ever reported in the ternary Nd-Fe-B system at room temperature for the $Nd_{150}Fe_{14}B$ samples. Thus, the magnetic interaction between single domain particle represents a key factor in determining coercivity of hard magnetic matters.

Contact: Kannan M. Krishnan, Lawrence Berkeley National Laboratory
Phone: (510) 486-4614, Fax: (510) 486-5888, E-mail: krishnan@lbl.gov

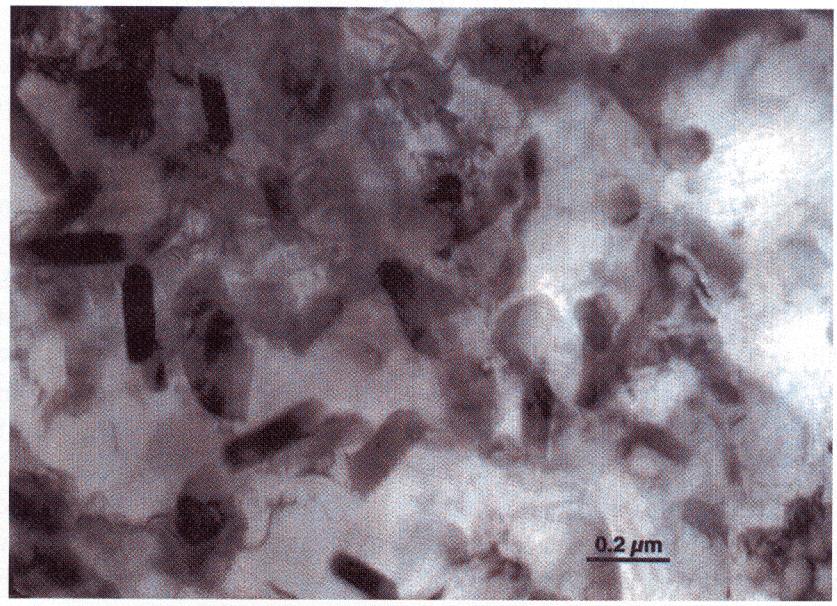

Figure 1. Microstructure of the annealed $Nd_{40.5}Fe_{14}B$ sample.

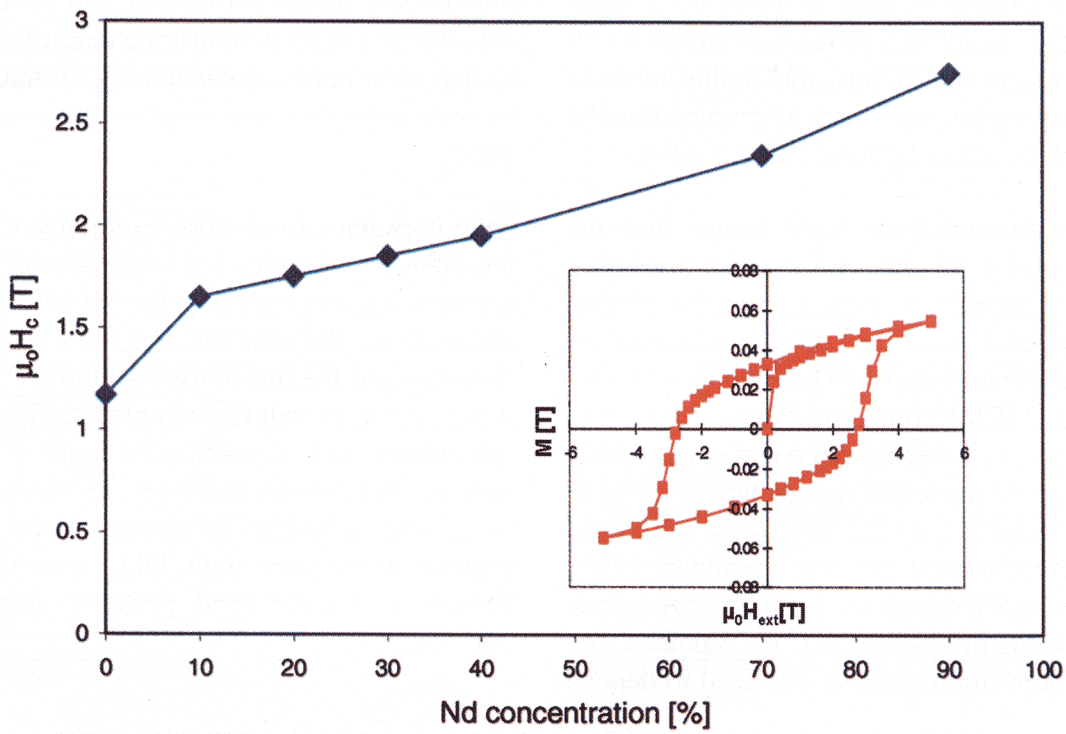

Figure 2. Dependence of coercivity of $Nd_xFe_{14}B$ as a function of the Nd-matrix concentration. Insert represents the MH loop of $Nd_{150}Fe_{14}B$.

Hard Coatings for Reduced Friction and Wear in Micro-Electromechanical Systems

J. W. Ager III, O. R. Monteiro, L. G. Brown, Lawrence Berkeley National Laboratory
D. M. Follstaedt, J. A. Knapp, M. T. Dugger, T. Christenson, Sandia National Laboratory

Motivation—"Micromachines" made with lithographically fabricated moving parts are an area of considerable current technological interest. Several applications involve the use of "microgears." These gears have several wear surfaces, including the gear faces, gear teeth, and the holes for their axles. The operating speed of some micromachines that use these gears exceeds 50,000 rpm, so that wear of critical contacting surfaces, such as the gear teeth, is of concern. In other applications, the machines must sit idle for extended periods of time. In this case, corrosion and stiction are of concern. In this Center for Excellence project we are concentrating on a subclass of Micro-Electromechanical Systems (MEMS) devices manufactured by the "LIGA" process. In LIGA, X-ray lithography is used to generate a high-aspect-ratio "mold" in a photoresist material. Ni metal is electroplated into the molds to form micron-sized parts, which are assembled into the final machine either by hand or by a robot.

Accomplishment—We have found that the application of a 30 - 70 nm hard carbon coating produces a significant reduction in the friction coefficient and wear rate of electroformed Ni substrates in reciprocating sliding contact under simulated MEMS operating conditions. To evaluate the performance of coated components, a series of 70-μm-thick microgears ranging in diameter from 0.2 to 2.2 mm were fabricated from electroformed Ni via standard LIGA processes and fixtured on posts in preparation for the coating procedure (Fig. 1). A pulsed vacuum-arc deposition process was used to deposit a carbon coating on the gears with the plasma incident at a shallow angle to the gears' top surface (Fig. 2). We used optimized deposition conditions to produce a coating (90 nm nominal thickness) with relatively low stress and good adhesion while maintaining high hardness. The coating process is known to be somewhat conformal to the component surfaces. The coating uniformity, particularly in the high-aspect-ratio areas between the gear teeth, was evaluated with micro-Raman spectroscopy (Fig. 3). The analysis showed that the coating was uniform in thickness on the top gear surface. Between the gear teeth (aspect ratio = 4) the coating was the same thickness as on top of the gear down to a point 50 μm below the top surface. Below that point (i.e. between 50 and 70 μm), the coating thickness is somewhat thinner, but is still present. These results demonstrate that it is possible to deposit a hard carbon coating on microgears to reduce friction and wear in micromachined gears.

Significance—Joint work within this Center of Excellence project has led to the development of a promising wear coating for MEMS actuators and motors. We conclude that, with appropriate fixturing and the use of the vacuum arc process, it is possible to coat the complex surfaces of the microgears with a continuous coating of hard carbon. We expect, based on our previous tests on coated substrates of electroformed Ni, that coating microgears with DLC should reduce friction and wear (and possibly stiction) in micromachines.

Contact: Joel W. Ager III, Lawrence Berkeley National Laboratory
Phone: (510) 486-6715, Fax: (510) 486-4114, E-mail: ager@lbl.gov

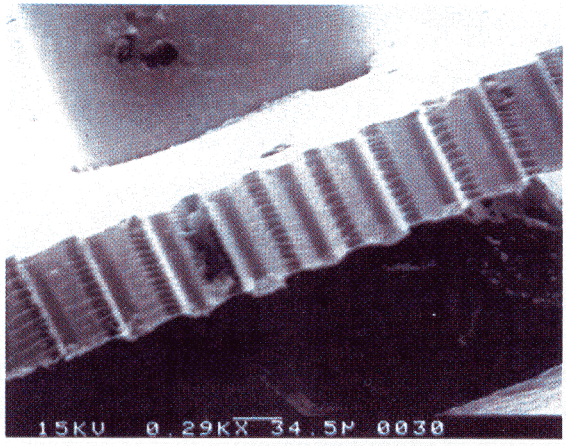

Figure 1. SEM micrograph of a 980 μm diameter gear, side view. The gear is 70 μm thick. The fixturing post can also be seen above the gear.

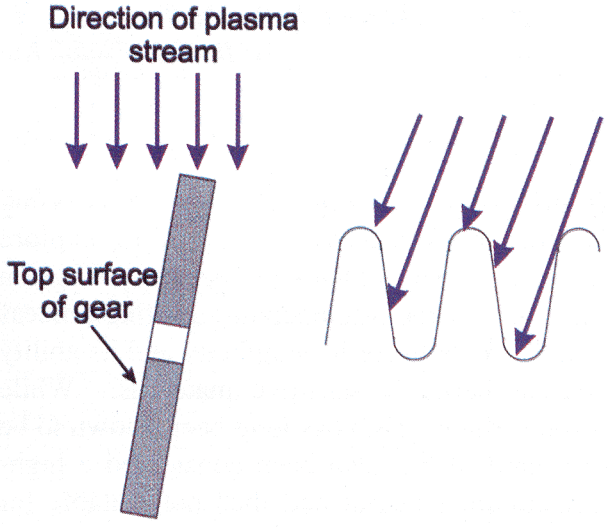

Figure 2. Schematic of deposition geometry. Left (side view): the plasma stream was oriented 80° to the surface normal. Right: schematic of shadowing. At the angle of incidence shown (20°), the area between the gear teeth is not fully in the line of sight of the plasma.

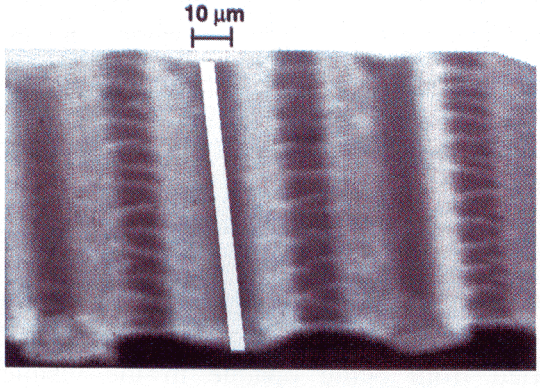

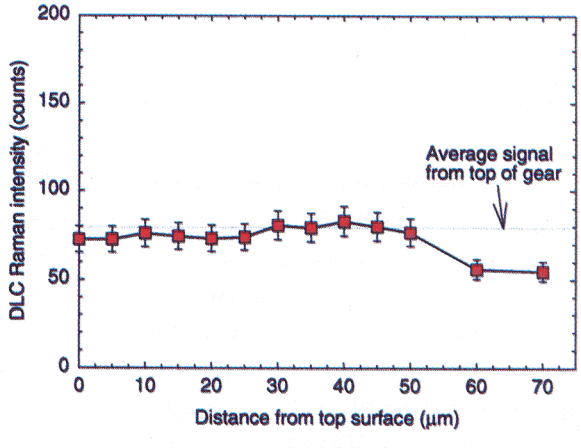

Figure 3. Left: SEM detail of area between gear teeth (magnified from above). The width of the Raman microprobe (5 μm) and the probed region are indicated by the white line. Right: Raman intensity between gear teeth as a function of distance from the top surface of the microgear. The intensity observed from scans on the top of the gear is indicated by the solid straight line.

Low-Temperature Process for Depositing Very Hard Boron Carbide Films

P. B. Mirkarimi, D. L. Medlin, and K. F. McCarty, Sandia National Laboratories, CA
D. B. Poker, Oak Ridge National Laboratories

Motivation—The objective of the Processing for Surface Hardness project is to explore processes to deposit hard, protective coatings on materials. A room-temperature coating process is desirable both for its simplicity and its ability to coat thermally sensitive materials. While boron carbide (B_4C) has long been known to be very hard, it has also been considered a high-temperature material and thus not suitable for low-temperature processing. To this end, we have explored development of a simple, low-temperature process to deposit B_4C films.

Accomplishment—We have developed a simple, low-temperature process to synthesize boron carbide (B_4C) coatings. Films were grown on silicon substrates by radio-frequency sputtering of a single B_4C target using a planar magnetron source and argon sputtering gas. We investigated the properties of the films as a function of substrate temperature and DC bias applied to the substrate. Film hardness was measured using a Nanoindenter instrument and the (analytic) Oliver-Pharr method. (Previous work within this project used finite-element analysis to show that the Oliver-Pharr method produces reasonably accurate hardness values for the hardness range under consideration here. However, the method can significantly underestimate the elastic modulus.) Figure A shows the film hardness as a function of growth temperature. Above 500°C, the deposited films have a hardness of about 35 GPa; in contrast, the hardness of a mild steel is about 2 GPa. The material made at 1000°C is crystalline B_4C, as evidenced by transmission electron microscopy (Fig. B) and Raman spectroscopy (Fig. C). As the growth temperature is reduced below 500°C, the hardness decreases (Fig. A) and the films become amorphous (Figs. C and D). Remarkably, however, by simply biasing the substrate at -25V during deposition, a film can be grown at room temperature that is as hard (> 35 GPa) as that grown at 1000°C.

Significance—A low-temperature process opens the door to coating temperature-sensitive materials such as polymers. Such materials cannot be coated using many current deposition technologies. In addition, our process is relatively simple, involving only a single sputtering target and a slightly biased substrate. In contrast, synthesis of titanium nitride coatings requires, for example, precise control over the nitrogen content in the sputtering system. Work by other participants in this project (see also following Brief) has investigated other boron-based coatings, including boron, boron suboxides, boron nitride, boron carbide, and boron phosphide. Within these boron-based materials, it is possible to "engineer" coatings with vastly different properties. For example, the hardness can be varied from about 1 to over 60 GPa, the lubricity can be changed from being unremarkable to being "self-lubricating," the electrical conductivity can be changed from insulating to conductive, and the optical bandgap can be varied from being opaque in the visible to transparent well beyond the visible spectrum.

Contact: Kevin McCarty, Sandia National Laboratory
Phone: (925) 294-2067, Fax: (925) 294-3231, E-mail: mccarty@sandia.gov

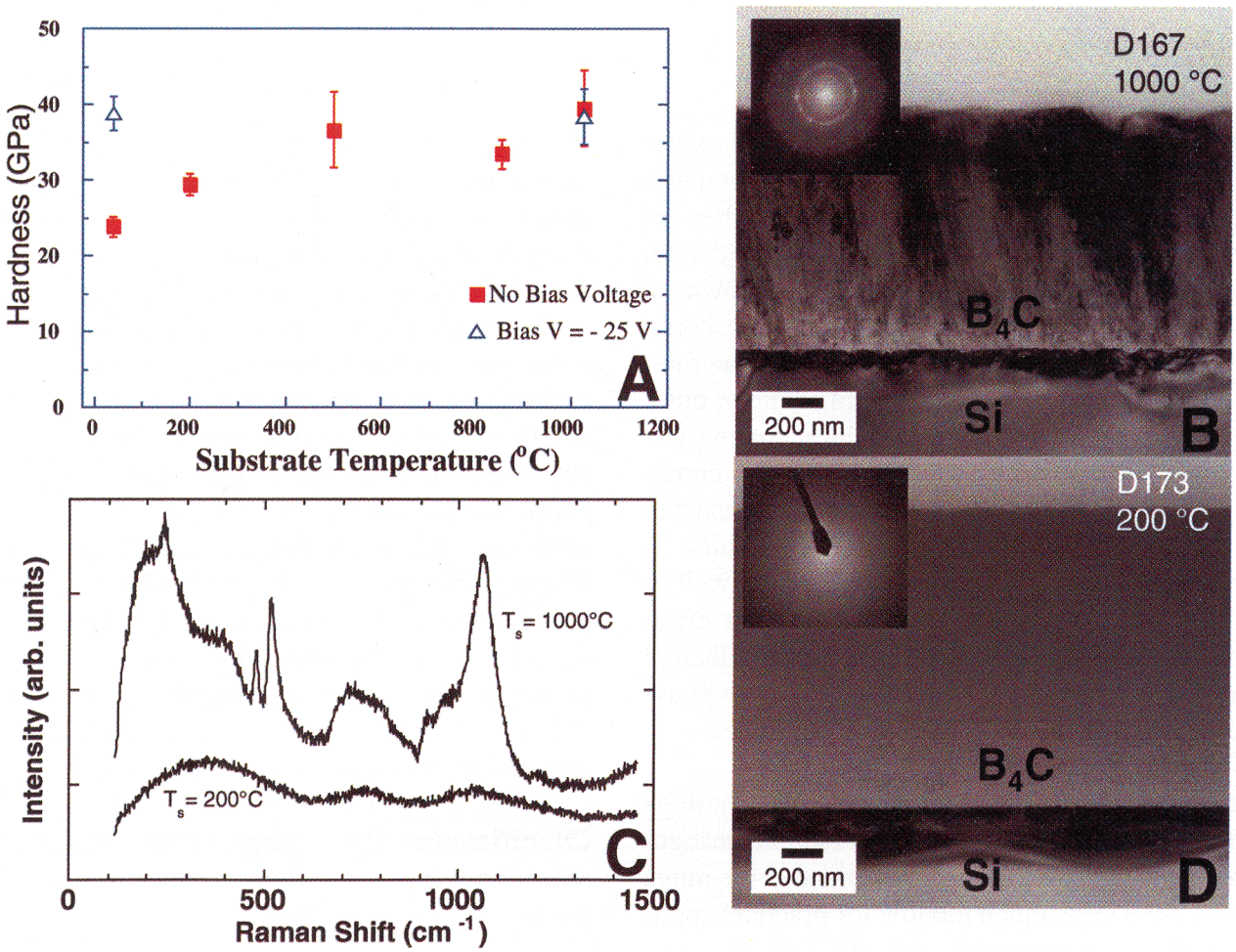

Figure 1. (A) Hardness of B_4C coating, measured using nanoindentation, as a function of substrate temperature and presence of electrical bias. (B) Cross-sectional transmission electron micrograph of B_4C film grown at 1000°C. The image contrast as well as the diffraction pattern (insert) show that the material is crystalline. (C) Raman spectra of B_4C films grown at 1000°C (upper) and 200°C (lower). The 1000°C-film exhibits the well-defined phonon scattering of crystalline B_4C, unlike the amorphous material made at 200°C. (D) Cross-sectional transmission electron micrograph of B_4C film grown at 200°C. The lack of any image contrast and the diffuse diffraction pattern (insert) show that the material is amorphous.

Hard Boron and Boron-Nitride Coatings

Alan Jankowski, Lawrence Livermore National Laboratory
David B. Poker, Oak Ridge National Laboratory

Motivation—Boron and its nitrides and oxides form an interesting class of materials, comparable to diamond in hardness. In addition, they are resistant to thermal and chemical degradation, and some forms have even been shown to scratch and wear a diamond tip. Cubic boron nitride is one of the harder members of the family, exhibiting excellent chemical stability, but it is not strongly adherent as a thick coating (>1 micron) and requires special processing conditions. The members of this boron family exist in phases that exhibit cubic bonding, which is responsible for the extreme hardness, as well as the softer hexagonal phase. This Center effort examines the prospect of transforming adherent and hard boron coatings to the cubic phase through the use of ion implantation.

Accomplishment—Boron nitride coatings deposited at room temperature exhibit hexagonal bonding and a surface hardness in the range of 0.7-0.9 GPa, much too low for practical applications. Implantation with 90 keV N+ ions induces a defect population that enhances the production of cubic bonding, as shown in Fig. 1. The surface hardness, as measured by a Berkovich-type nanoindenter, increased to 3 GPa (Fig. 2). (Note that the film hardness is reflected in the measurements taken at the lowest depths. Greater depths indicate the hardness of the silicon substrate, about 10 GPa.) Implanting at the higher energy of 180 keV induces the opposite effect on hardness, a softening to about 0.2 GPa, indicating an extreme sensitivity of the hardening or softening of the as-deposited boron nitride on the implantion conditions. Similar implantation of pure boron is found to increase the hardness to 40 GPa, nearly the value for cubic boron nitride. It is concluded that nitrogen implantation of pure boron and hexagonal boron nitride is similar to processes such as ion-beam assisted deposition, where stabilization of the cubic phase is produced during growth by the ion beam. However, in contrast to the deposition process, which produces poor adhesion, implantation of an already-adherent hexagonal boron nitride phase does not lead to reduced adhesion.

Significance—Any application requiring reduction in friction and wear is a candidate for the use of these materials. Examples include power generation, machining, magnetic data storage, and optical devices. These materials represent an alternative to amorphous hard carbon, which has already become widely used in the microelectronics industry for hard disk coatings. Development of adherent, durable coatings of boron and its nitrides will provide similar advantages.

Contact: Alan Jankowski, Lawrence Livermore National Laboratory
Phone: (925) 423-2519, Fax: (925) 422-0049, E-mail: jankowski1@llnl.gov

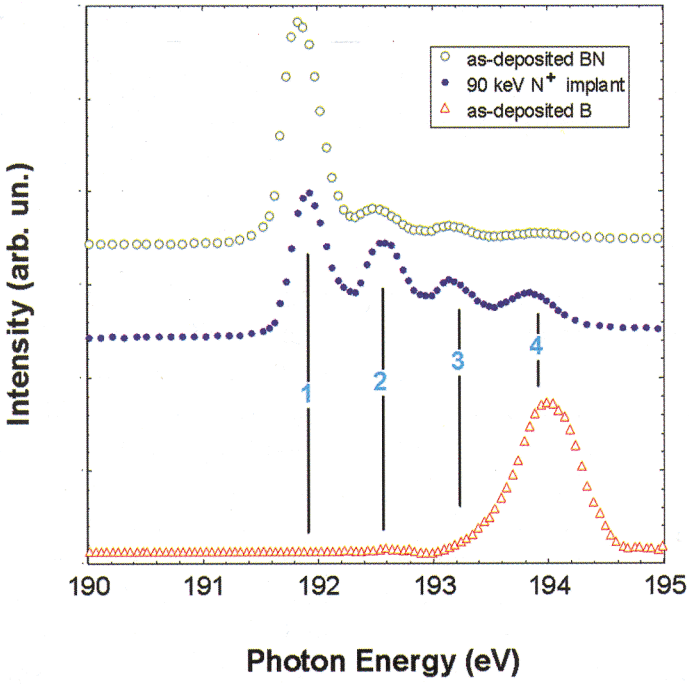

Figure 1. Near edge x-ray absorption fine structure (NEXAFS) analysis of boron (open triangles), as-deposited boron nitride (open circles), and N+ implanted boron nitride (closed circles). Implantation reduces the population of hexagonal bonding (#1) reflected by the as-deposited spectrum while increasing the cubic bonding (#4) as seen in the boron spectrum.

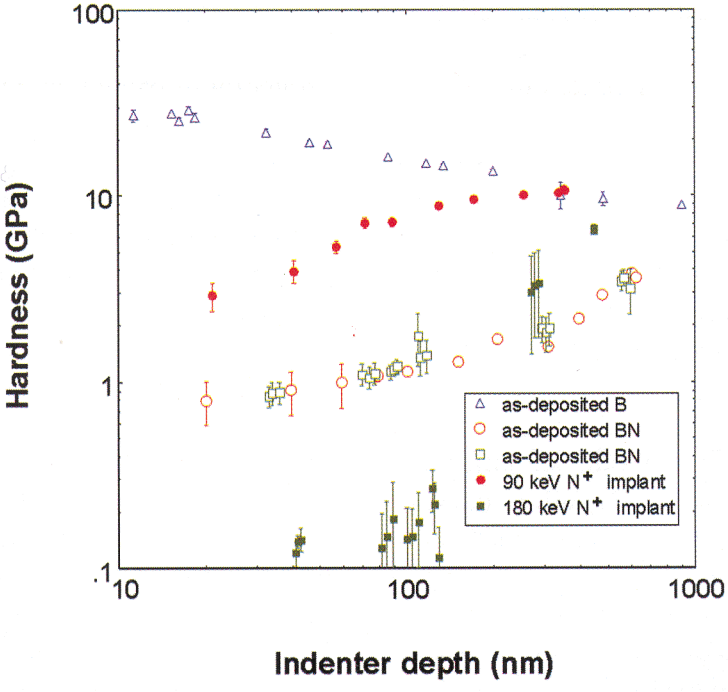

Figure 2. Surface hardness of as-deposited hexagonal boron nitride (open circles and squares), boron nitride implanted with 90 keV N (closed circles), boron nitride implanted with 180 keV N (closed squares), and pure boron (open triangles), for comparison. The 90 keV N-implanted samples exhibited a pronounced increase in hardness, while the 180 keV N-implanted samples actually decreased in hardness, suggesting that the implant conditions are critical.

Sulfur Segregation and Al_2O_3 Scale Adhesion

P. Y. Hou, Lawrence Berkeley National Laboratory
K. B. Alexander, Oak Ridge National Laboratory
J. L. Smialek, NASA Lewis Research Center

Motivation—The addition of reactive elements (RE's), such as Y, Hf, Ce and Zr, is known to increase the adherence of Al_2O_3 scales to underlying alloys. A widely accepted mechanism is that the REs getter the sulfur impurity in the alloy, thus preventing it from segregating to the scale/alloy interface to weaken the interfacial bonding. Although there has been some debate whether the large and negatively charged sulfur ion would segregate to an intact oxide/metal interface, ample evidences exist from Auger and analytical electron microscopy studies that sulfur is indeed present at static and growing oxide/metal interfaces. Its effect on oxide scale adhesion, however, has not been directly demonstrated. Indirect experimental evidence of the detrimental effect of sulfur on scale adhesion has been provided by the oxidation of desulfurized alloys and their ability to retain the scale under severe thermal cycling conditions.

The purpose of this study was to relate the amount of sulfur at the Al_2O_3/alloy interface to the spallation resistance of the scale, whether during cooling or under externally applied loads. Fe-28Al-5Cr (at. %) alloys, with or without a Zr addition or a desulfurization H_2-anneal were used.

Accomplishment—The amount of sulfur segregated to the growing Al_2O_3/alloy interface was studied using Auger electron microscopy after the scale was removed by scratching in ultra high vacuum. Scale adhesion was compared from the degree of scratch-induced spallation. Sulfur was found to slowly segregate to the growing scale/alloy interface of the untreated alloy, but was not found at the interface of the Zr-containing or the H_2-annealed alloys. Scale adhesion was extremely poor for the untreated alloy, showing complete spallation after the scale thickness reached about 0.5 μm. Thinner scales did not show any spallation during cooling, but adhesive failure and spallation to the scale/alloy interface could be easily achieved by scratching. Annealing the alloy with H_2 to remove its indigenous sulfur impurity greatly improved scale adhesion. Spallation only took place sporadically in small areas after the scale had thickened to greater than 1 μm. However, scratching the oxide surface could still cause extensive spalling. Unlike any of the above behavior, the Zr-containing alloy never showed any spontaneous spallation during cooling. Adhesive failure was difficult to induce under applied loads. Instead, stresses were released by numerous through-scale cracks, which did not lead to delamination and spallation as in the case of the Zr-free alloy. This behavior indicates a very strong scale/alloy interface.

Significance—There is now strong evidence that not all S-free interfaces are strong. Although eliminating the sulfur in the alloy can greatly improve scale adhesion, the presence of reactive elements clearly has additional beneficial effects related to making the scale-alloy interface even stronger. This shows that the role of the reactive elements is more than that of an impurity scavenger. It also raises a fundamental question whether all thermally grown oxide-metal interfaces are intrinsically strong, and whether it is only the segregation of impurities, particularly sulfur, that makes them weak.

Research sponsored by the Division of Materials Sciences, Office of Science and the Office of Fossil Energy, U. S. Department of Energy. and the Electric Power Research Institute.

Contact: Peggy Hou, Lawrence Berkeley National Laboratory
Phone: (510) 486-5560, Fax: (510) 486-4995, E-mail: pyhou@lbl.gov

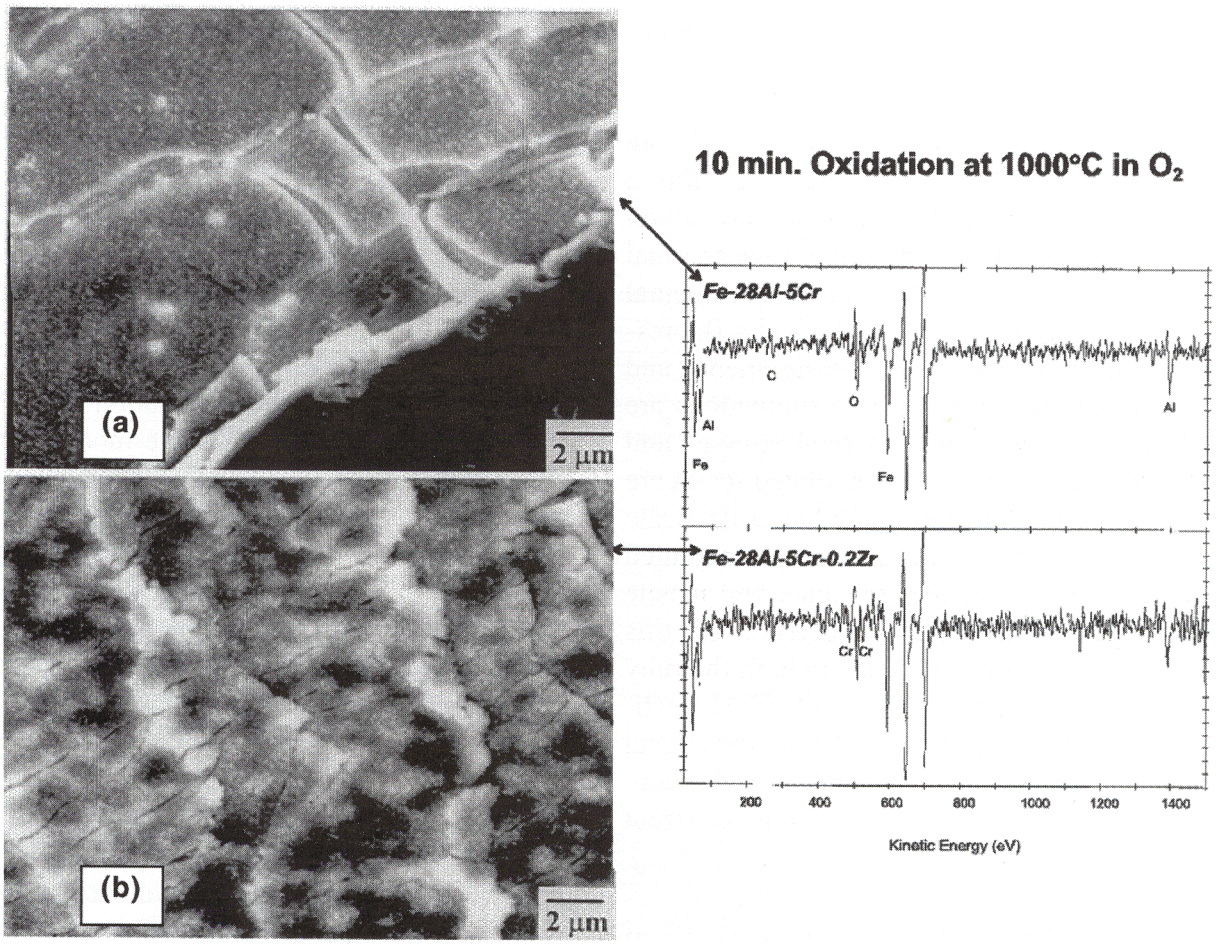

Figure 1. Not all low-sulfur alumina-alloy interfaces are strong. Even when Auger spectroscopy showed that both Fe-Al-Cr and Fe-Al-Cr-Zr metal-oxide interfaces were sulfur-free, the alumina film on the first alloy spontaneously spalled upon application of a scratching load (a) while the oxide on the latter substrate remained adherent (b).

Residual Stresses in Convoluted Alumina Scales

J. K. Wright, R. L. Williamson, Idaho National Engineering and Environmental Laboratory
D. Renusch, M. Grimsditch, B. W. Veal, Argonne National Laboratory
P. Y. Hou, R. M. Cannon, Lawrence Berkeley Laboratory

Motivation—Alumina scales that grow during oxidation of FeCrAl alloys can develop a convoluted morphology. Although convolution relieves the overall growth stress, high thermal stresses develop locally and can be detrimental to the scale or interface integrity. Ruby fluorescence (piezospectroscopic) measurements and finite element modeling (FEM) simulations are used to examine residual thermal stresses and strains that result when the convoluted scales are cooled to room temperature. Unlike a flat scale that is in biaxial compression, a convoluted scale contains significant gradients and tensile stress components. The objectives of this research are to gain confidence in both the ruby fluorescence measurements and FEM techniques via their comparison, to better understand surface oxide failure mechanisms, and ultimately to provide criteria for design of more adherent oxides.

Accomplishment—A Fe-18wt%Cr-5wt%Al specimen was oxidized at 1000°C for 3 h, producing a 1 μm-thick convoluted α-Al_2O_3 scale (Fig. 1a & b). The residual stress was measured across individual convolutions using ruby fluorescence with μm-level spatial resolution (Fig. 1c). FEM was used to compute the residual stresses and strains during simulated cooling (Fig 1d&e). The convoluted morphology was simplified to a two dimensional sinusoidal shape based on topography measurements. Good agreement was found between the experiments and modeling, with both showing a systematic reduction in hydrostatic stress towards the peaks of the convolutions. While the hydrostatic stresses are compressive throughout the scale, modeling indicates local tensile stress components in the peak of convolutions both near the free surface and the interface.

Significance—The high tensile stresses at the scale/metal interface and within the top portion of the scale at the peak of the convolution can cause scale separation at the interface or scale cracking at the surface. Both types of failure are often found in oxidation studies. Tensile components can also facilitate void formation, which may then act as crack initiation sites upon cooling. Any offset between the model curves and experimental data could be an indication of growth stresses present in the sample, which are not considered in the model. The small offset appears to be within measurement error and suggests that while growth stresses are large enough to cause convolutions to form at the oxidation temperature, they are minimal compared to the thermally-generated stresses. As a stress measurement technique, ruby fluorescence is well suited for measuring the effects of a convoluted geometry. Because the ruby fluorescence technique provides only the hydrostatic stress averaged over an excited volume that includes the entire alumina scale thickness, a lower hydrostatic stress is measured where the local tensile stress is actually the most severe. Thus, the technique is limited in its ability to predict specific failure locations and to measure stress gradients through the scale thickness. The FEM analysis, on the other hand, provides detailed information about all stress and strain components, plasticity effects, and gradients, and proves very useful in providing an increased understanding of the complex mechanical response during cooling. However without the experimental results providing much needed verification of the model assumptions and approximations, their impact is diminished.

Research sponsored by the Division of Materials Sciences, Office of Science and the Office of Fossil Energy, U. S. Department of Energy.

Contact: Jill Wright, Idaho National Engineering and Environmental Laboratory
Phone: (208) 526-9723, Fax: (208) 526-0690, E-mail: jk3@inel.gov

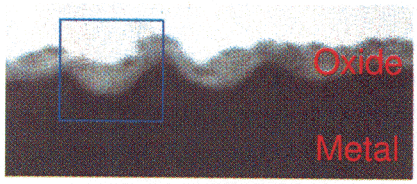

(a) sample cross-section showing the convoluted α-Al_2O_3 scale

(b) sample top view

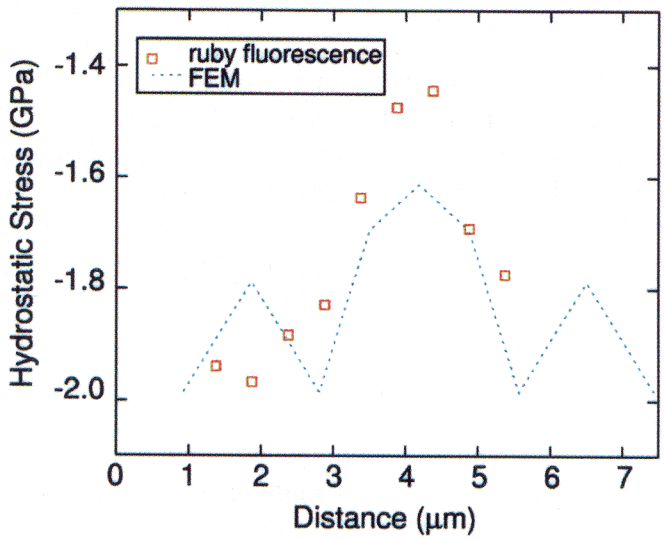

(c) comparison of measured and modeled hydrostatic stress

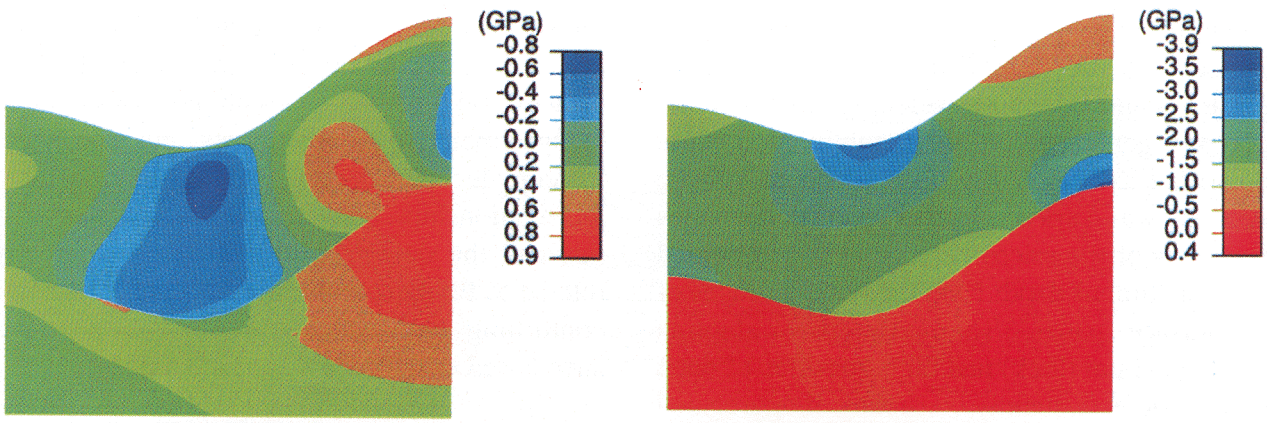

(d) (e)

Figure 1. Hydrostatic stresses in a convoluted Al_2O_3 scale on FeCrAl samples (a,b) were modeled and measured. Although good agreement was found (c), stress gradients and regions of high local tensile stress (d) are not apparent from the hydrostatic stress (e) which in measurements are effectively averaged over the excited volume.

The Use of Positrons to Probe the Defect Structures of Protective Alumina Films

B. Somieski, L. D. Hulett, J. Xu, B. A. Pint, and P. F. Tortorelli, Oak Ridge National Laboratory

Motivation—Thermally grown oxide scales can provide high-temperature oxidation protection if they are slow-growing, sound, and adherent to the substrate. Defect structures of these scales control the diffusion processes involved in their growth and, as such, also influence the development of stresses and their mechanical integrity. Positron spectroscopy can serve as an useful nondestructive characterization tool in examining the processes by which defects such as mono- and di-vacancies, vacancy clusters, and dislocations develop in an oxide film as a function of substrate variations and growth/oxidation conditions. This approach can be particularly valuable for oxide layers because stress or interstitial impurities do not contribute to the uncertainty in determining defect structures by positron spectroscopy. Despite the potential advantage of using positrons to probe the micro-defect structure of protective oxide films, little work in this area has been performed.

Accomplishment—Positron spectroscopy of thermally grown alumina on iron and nickel aluminides was used to determine the utility of the technique to characterize the defect structures of protective oxide scales (Fig. 1). Lifetimes of the positrons and Doppler broadening of the gamma photons generated by their annihilation were measured as the energy with which they were injected was varied. In this manner, densities and sizes of the micro-defects were determined as a function of depth from the outer surfaces of the surface oxides. Thermally grown alumina scales (1-2 μm thick) had high densities of open volume defects, mainly consisting of aggregated vacancies. The thermally grown alumina on iron aluminide had a uniform through-thickness defect distribution. This was not the case for the scale on the nickel aluminide: the average defect (vacancy cluster) size increased as a function of depth into the alumina film grown on this substrate. These observed differences in the defect structures of the films grown on the two aluminides may reflect variations in doping levels in the respective oxide layers as well as an effect of scale microstructure. Furthermore, positron spectroscopy showed that the defect structures of the substrates near the oxide-metal interfaces were significantly changed; high densities of vacancies were detected. Detailed defect analyses of these specimens were included in a paper accepted for publication in Physical Review B: "Microstructure of Thermally Grown and Deposited Alumina Films Probed With Positrons" by B. Somieski, L. D. Hulett, J. Xu, B. A. Pint, P. F. Tortorelli, B. Nielsen, P. Asoka-Kumar, R. Suzuki, and T. Ohdaira

Significance—The results of this study indicated that positron spectroscopy can be an effective tool in [1] characterizing defect types and their distribution in alumina films and scales, [2] examining the influence of dopants in the alumina scales on the defect structure, and [3] determining changes in substrate defect distributions due to diffusion processes associated with oxide growth. When combined with judicious choices of specimens and experiments, positron spectroscopy techniques can yield information about the relationships between substrate characteristics and the defect structures that are directly related to fundamental mass transport processes controlling high-temperature oxidation resistance based on protective surface oxides.

Research sponsored by the Division of Materials Sciences, Office of Science and the Office of Fossil Energy, U. S. Department of Energy.

Contact: Peter Tortorelli, Oak Ridge National Laboratory
Phone: (423) 574-5119, Fax: (423) 241-0215, E-mail: tortorellipf@ornl.gov

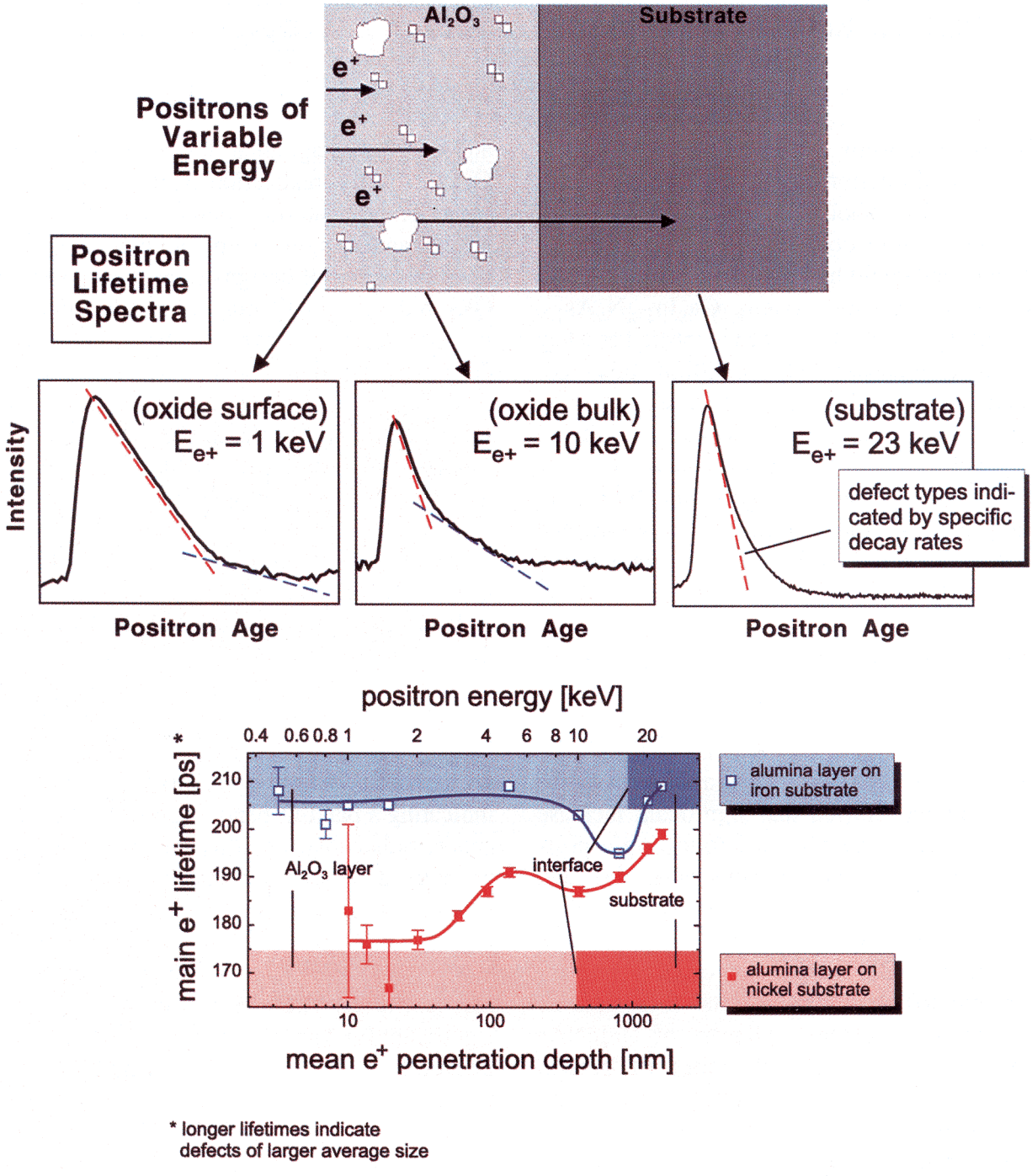

Figure 1. Defect densities and sizes as a function of depth from the outer surfaces of surface alumina were determined from using positrons of variable energy and measuring lifetimes and Doppler broadening of the gamma photons generated by their annihilation.

GaInNAs: Photovoltaic Material

A. A. Allerman[1], D. J. Friedman[2], J. F. Geisz[2], E. D. Jones[1], Y. H. Kao[3], Sarah R. Kurtz[2],
Steven R. Kurtz[1], A. Mascarenhas[2], N. A. Modine[1], J. M. Olson[2], J. D. Perkins[2],
W. Walukiewicz[4], A. F. Wright[1]
[1]SNL [2]NREL [3]SUNY [4]LBL

Motivation—For future-generation GaAs-based multijunction solar cells, efficiencies exceeding 40% should be achievable if a suitable GaAs-compatible semiconductor with a 1 eV band gap could be identified (Fig. 1). A new semiconductor alloy system, $Ga_xIn_{1-x}N_yAs_{1-y}$ (hereafter GaInNAs) has been identified as a key candidate material. The addition of small amounts of nitrogen to the GaInAs alloy system greatly reduces the band gap energy, with N concentrations of ~3% yielding band gaps of 1 eV. Furthermore, at the appropriate In/N concentration ratio, the material is lattice-matched to GaAs, avoiding the inherent problems found in strained material.

Accomplishment—Initial work on the growth of this alloy quickly yielded material lattice-matched to GaAs and with the desired band gap of 1 eV at ~2% N, 6% As. Studies of the photoluminescence (PL) line widths and intensity for these samples showed that significant increase in PL intensity was obtained following a post-growth anneal. When solar cells were fabricated from the as-grown (unannealed) material, they were found to have very poor internal quantum efficiencies (QEs), on the order of 20%, compared to the >90% required (Fig. 2a). To examine this problem, epilayers of GaInNAs were grown under a wide range of growth conditions, and their carrier mobilities and photoelectrochemical-junction spectral responses were characterized. The spectral response was found to increase with decreasing carrier density, implying that diffusion lengths in this material are very short and that collection of photogenerated carriers is accomplished by field aided collection in the junction depletion region. Consistent with this, the mobility measurements showed that mobilities in GaInNAs are at least an order of magnitude lower than in GaAs. Guided by the realization of the problem with the as-grown material, counter-doping and post-growth annealing were applied in the next iterations of solar cell designs to produce cells with QEs in the 60%-70% range (Fig. 2b). While this is much improved over the first attempts, the desired >90% QEs have not been obtained. Also, open-circuit voltages for these devices are only ~0.3V, about half of the ideally-expected value, reflecting high dark currents due presumably to high recombination in the junction.

Thus, basic studies of the structural and electronic properties are of compelling practical as well as fundamental interest. EXAFS studies of the alloy showed that the nitrogen sits substitutionally in an arsenic site, as would be expected in the ideal case. The pressure dependence of the band gap was measured by PL and compared with first-principles calculations (Fig. 3), indicating a band-to-band origin of the luminescence, rather than impurity behavior. However, pressure-dependent photo-modulation spectroscopy (Fig. 4) and atmospheric-pressure electro-reflectance spectroscopy studies of the alloy showed evidence of a nitrogen-associated resonant level. The presence of this level is of significant fundamental interest; it also provides a natural explanation for the low mobilities/lifetimes limiting the performance of devices made to date with GaInNAs

Significance—With these studies, significant progress has been made in understanding the issues involved in achieving ultrahigh-efficiency solar cells to satisfy the demands of the booming space-photovoltaics industry as well as the emerging terrestrial high-concentration photovoltaics market.

Contact: S. K. Deb, National Renewable Energy Laboratory
Phone: (303) 384-6405, Fax: (303) 384-6481, E-mail: satyen_deb@nrel.gov

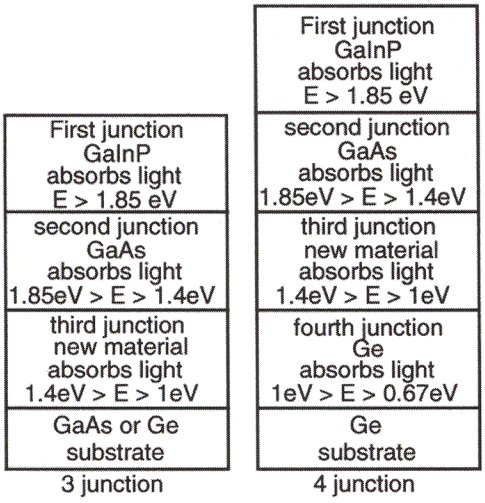

Figure 1. Future-generation 3- and 4-junction multijunction solar cell structures with projected efficiencies in excess of 40%

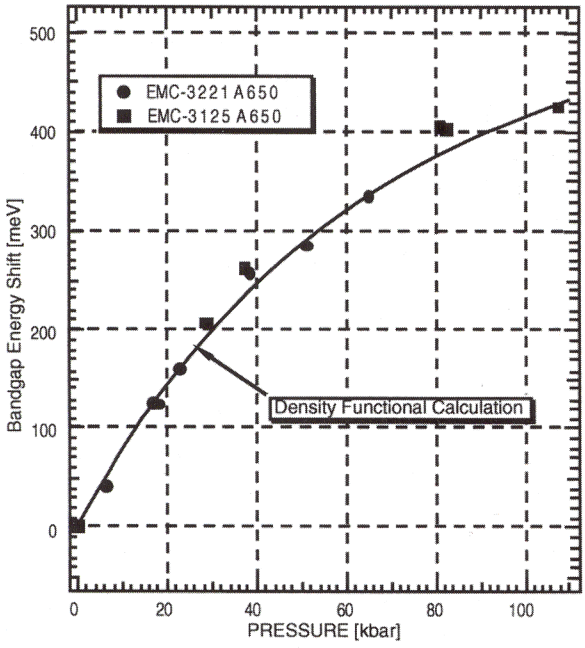

Figure 3. Experimental and theoretical comparisons of the change in the low temperature band gap energy vs pressure. [Jones, Allerman et al, SNL]

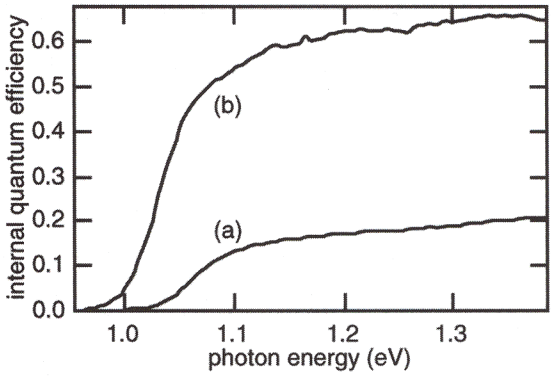

Figure 2. Quantum efficiencies for GaInNAs solar cells with (a) conventionally grown base, and (b) counterdoped base. Similar improvements in quantum efficiency were also achieved by post-growth annealing. [NREL; J. Cryst. Gr. **195**, 409 (1988)]

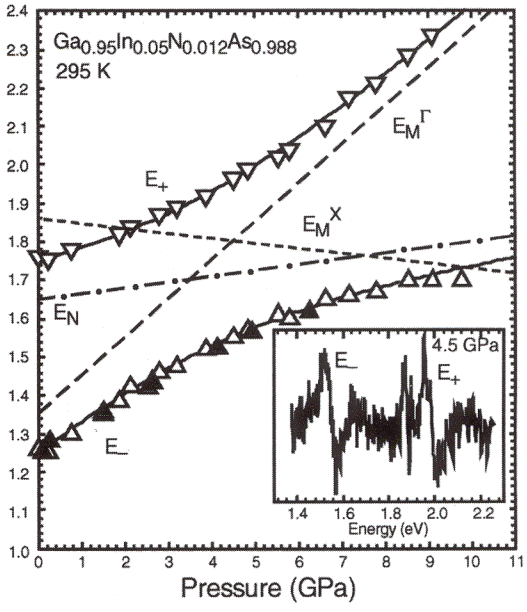

Figure 4. Change of the E_- and E_+ transition energies in $Ga_{0.95}In_{0.05}N_{0.012}As_{0.988}$ as a function of applied pressure. The open and closed triangles are photomodulated reflectance and transmission data, respectively. The dashed, dotted, and dot-dashed lines are the pressure dependence of the Γ and X conduction-band edges of $Ga_{0.95}In_{0.05}As$ matrix and the N level relative to the top of the valence band, respectively. The inset shows a PR spectrum taken at 4.5 GPa. [Shan, Walukiewicz, et al, LBL; to be published in Phys. Rev. Lett]

Low-Temperature Grain Enhancement in Thin Silicon Films

***Bhushan Sopori, Wei Chen**, National Renewable Energy Laboratory*
***Teh Tan**, Duke University*

Motivation—Thin-film silicon solar cells have potential to yield high efficiencies even with low-quality material, thus offering a significant cost advantage over the thicker wafer-based cells. Theoretical calculations show that 18%-efficient cells can be obtained with substrate material similar in quality to that of current commercial cells. However, the realization of thin-film Si cells poses many challenges in cell design and fabrication. A suitable cell design must increase the light absorption by effective light trapping, while the cell structure should be easily amenable to impurity gettering and defect passivation. The challenges in cell fabrication are to make a large-grain, thin-Si film of good material quality on a low-cost substrate, and process this film into a solar cell at low temperatures. Conventional cell processing methods lead to problems arising from thermal mismatch between the Si and the substrate, impurity in-diffusion from the substrate to the Si film at high processing temperatures, and high process costs.

Accomplishment—We designed a single-junction thin-film Si cell that has many new features - both in the design and in the fabrication of the cell. The cell design is based on rigorous theoretical considerations, and is aimed at attaining an efficiency reaching 18%. Figure 1 illustrates the cell configuration. The major features of the cell are textured interfaces and a metal layer (consisting of Al/Cr) between the glass substrate and the Si film that performs several functions: it acts as a back reflecting electrode, as a stress relief layer, and participates in the grain growth process. An important consideration in the cell design is to minimize the cell thickness while minimizing the optical loss because of metallic absorption; this optical loss reduces the photocurrent of the cell. Figure 2 shows the maximum achievable current density of the cell as a function of cell thickness that takes into account the metallic loss. The results are given for a number of interface configurations. Our design calculations show that the grain size needed to achieve high efficiency is between 20-50 μm.

The main process steps required in the cell fabrication have been verified. We have been able to obtain large-grain films, from a-Si depositions, by a two-step grain growth and enhancement. The first step takes advantage of metal-induced crystallization caused by a thin layer of Al. The deposited film is a microcrystalline Si film with a grain size in the range of 0.1 to 0.5 μm. The second step consists of optically assisted grain enhancement at a low temperature-typically less than 550°C. This is a rapid process and, typically, yields grain sizes of 10-20 μm, as shown by the TEM micrograph of Figure 3.

Significance—A new cell design and the low-temperature processing steps for fabricating such a cell have been developed. The device structure and the process steps are aimed at realizing high efficiency, low-cost energy conversion. The defect engineering concepts have been applied to develop large-grain Si films. The device has the built-in structure for gettering impurities away from the active film and for very efficient optical confinement of the solar energy. All process steps are commercially compatible. When all the process steps are integrated, Si-based, high-efficiency thin film solar cells can be fabricated at a low cost. The grain enhancement process that we have developed entails very intriguing science that has many other applications.

Contact: S. K. Deb, National Renewable Energy Laboratory
Phone: (303) 384-6405, Fax: (303) 384-6481, E-mail: satyen_deb@nrel.gov

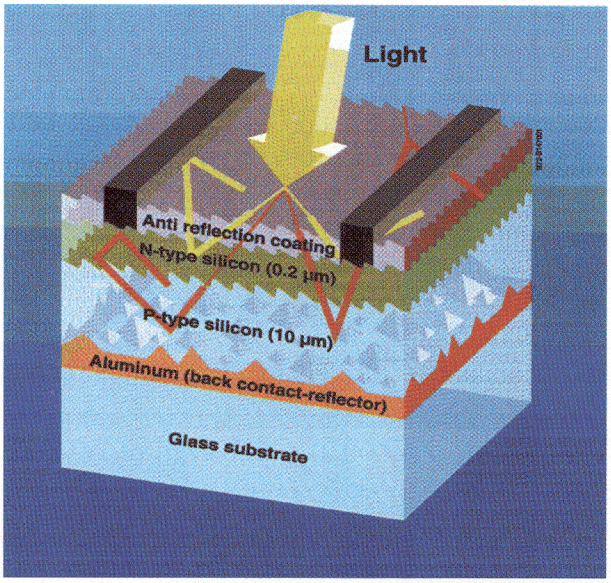

Figure 1. A schematic of a single-junction thin-film Si solar cell.

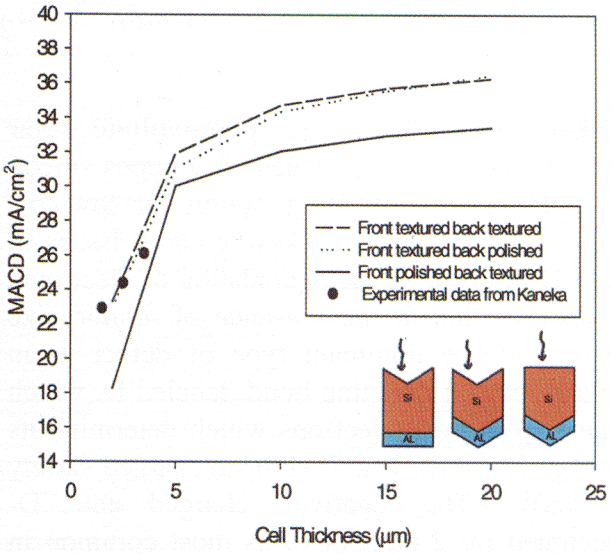

Figure 2. Calculated results showing maximum achievable (photo) current density (MACD) for various cell configurations. Also shown are the results from Kaneka from their cells.

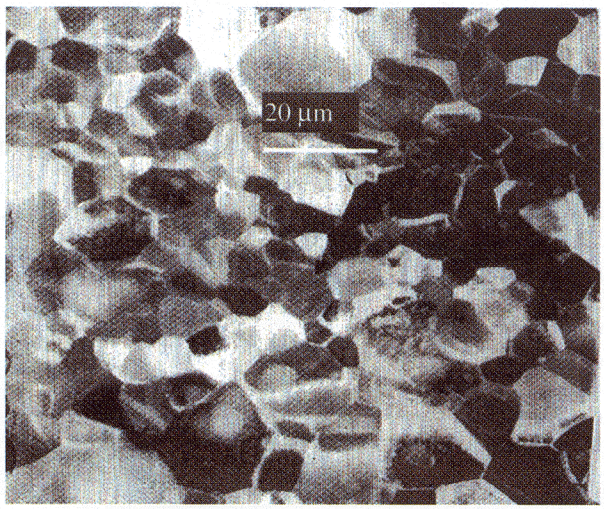

Figure 3. A TEM micrograph showing grain size of a thin-Si film after grain enhancement.

Positron Annihilation for Understanding Amorphous Si

Marc H. Weber, Mihail P. Petkov, and Kelvin G. Lynn, Dept. of Physics, Washington State Univ.,
Richard S. Crandall, National Renewable Energy Laboratory,
Vinita j. Ghosh, Brookhaven National Laboratory,

Motivation—Thin film photovoltaic solar cells based on hydrogenated amorphous silicon (a-Si:H) are a promising option for low-cost solar cells. One of the key research issues in a-Si:H thin film is the degradation of electronic properties due to the presence of atomic size defects. The dominant type of defect is an amphoteric Si dangling bond, labeled D, which can trap up to 2 electrons which determine its charge. In intrinsic a-Si:H the uncharged variety prevails. The negatively charged state, D- occupied by 2 electrons - is most common in n-doped a-Si:H. Based on electron spin resonance and other measurements, two atomic scale configurations were suggested to describe the latter in phosphorous (P)-doped a-Si:H: an isolated D- or a P-D- complex (*D-). In *D-, a P atom sits next to a-Si atom with a dangling bond. Direct experimental confirmation and theoretical modeling is needed to confirm or discard these suggestions.

Accomplishment—By using a surface-emitting semiconductor, we have used positrons to obtain significant information about the location and charge of the D in a-Si:H solar cells. Positrons seek out negatively charged (D-) or neutral D, get trapped, and eventually annihilate with an electron sitting in or near the D to produce a pair of gamma rays. These emitted photons give a "fingerprint" that allows the identification of atoms sitting next to a positron trap. Figure 1 shows such a fingerprint spectrum of a D- in the P doped region of a solar cell. This directly correlates to theoretical models of the defect and makes the first experimental identification of this P-D- complex. This was confirmed by theoretical calculations of positron annihilations in a-Si:H, where one of the atoms has a dangling bond as shown in Fig. 2. The positron wave function (small probability = blue, large = red) in the vicinity of the dangling bond Si (in green, other Si atoms in red) is enhanced by about 10% compared to the vicinity of the other Si atoms.

Significance—Positrons provide a new and important way to explore defects in a-Si:H. The quantitative information derived from positron annihilation, such as the first identification of the P-D- complex can be used to refine molecular dynamics simulations of a-Si:H and its defects. This should inevitably lead to a better understanding of a-Si:H structure and electronic properties. Besides the scientific impact of this new knowledge, the technological impact will stem from putting the fundamental knowledge to use in improving solar cells.

Contact: S. K. Deb, National Renewable Energy Laboratory
Phone: (303) 384-6405, Fax: (303) 384-6481, E-mail: satyen_deb@nrel.gov

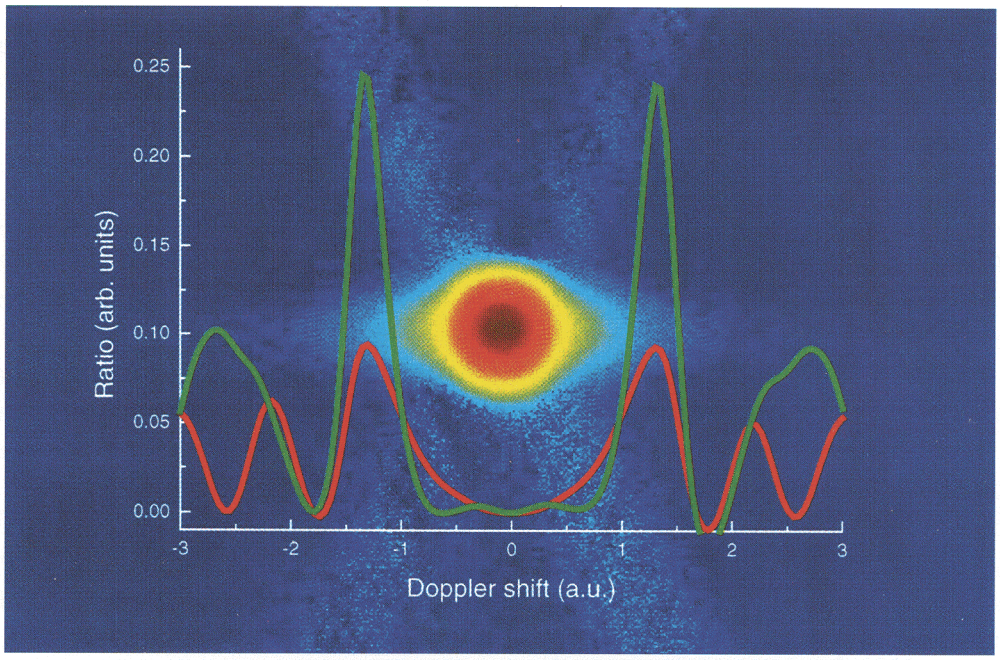

Figure 1. Fingerprint spectrum of a P-D_complex in a-Si:H.

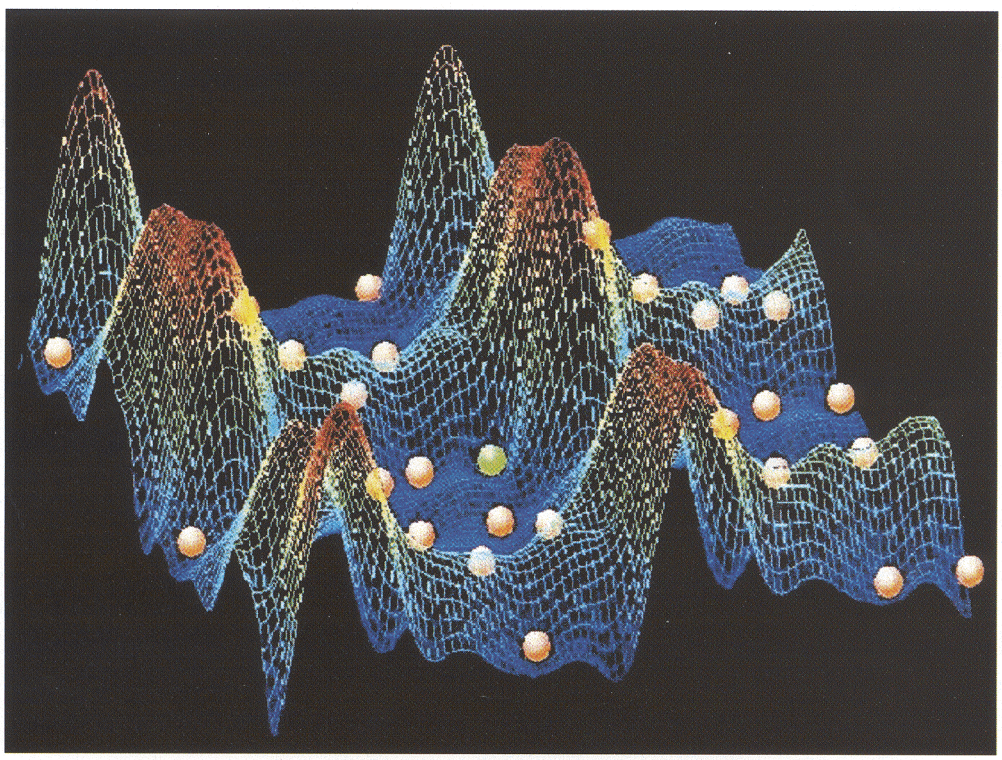

Figure 2. Simulation of positron wave function localized by dangling bond.

Thermal Expansion of Mo_5SiB_2: Theory and Experiment

C. L. Fu, C. M. Hoffmann, Claudia Rawn, J. H. Schneibel, and C. R. Hubbard,
Oak Ridge National Laboratory

Motivation—The coefficients of thermal expansion (CTE) for binary 5-3 transition-metal silicides are generally found to be highly anisotropic in the **a** and **c** directions. During the synthesis and processing of polycrystals of these materials, microcracking is therefore often observed. The addition of boron in Mo-Si changes the crystal structure from $D8_m$ (T1 phase; Mo_5Si_3) to $D8_l$ (T2 phase; Mo_5SiB_2) and substantially improves the oxidation resistance. An important basic question is whether or not the CTE anisotropy of the T1 phase is retained in the T2 phase. We address this question by both first-principles calculations and neutron powder diffraction measurements. This work is complemented by related studies in this Center project as described in the accompanying Briefs.

Accomplishment—Our first-principles calculations provide understanding at an atomistic level of the intrinsic strength and thermoelastic behavior of Mo-Si alloys. In previous work we have shown that the CTE anisotropy in Mo_5Si_3 is due to the combination of elastically more rigid basal plane and a higher anharmonicity along the c-axis. For Mo_5SiB_2, the elastic moduli are higher than those of Mo_5Si_3 (c. f., Table 1). This increase is partly attributed to the formation of Mo-B covalent bonds (an example is shown in Fig. 1). While the calculated elastic constants for the T2 phase still indicate that the basal plane is elastically more rigid than the c-axis (C_{11}+C12 > C_{33}), the effect of this difference on the CTE is balanced by a substantial increase of the elastic coupling (C_{13}) between the basal plane and c-axis. Most significantly, the lattice anharmonicity for the T2 phase is found to be nearly isotropic in the [100] and [001] directions (with Grüneisen constants 2.05 and 1.98, respectively). We identify this near isotropy in lattice anharmonicity as being due to the absence of directionally-bonded [001] chain structure characteristic of the T1 phase. As a result of decreased anisotropy in both the static (elastic) contribution and lattice anharmonicity as compared to the T1 phase, the CTE for the T2 phase become nearly isotropic in the a and c directions with the CTE in the a direction being slightly larger. The calculated CTE for the T2 phase are presented in Fig. 2.

The neutron powder diffraction experiments were carried out with powders made from arc-cast buttons of Mo_5SiB_2 annealed for 12 h at 2000°C (which results in nearly single T2 phase). The CTE were measured from room temperature to 1400°C. We find good agreement between theory and experiment. The experiment confirms the theoretical prediction of a nearly isotropic CTE for Mo_5SiB_2.

Significance—To eliminate the thermal stresses in polycrystalline materials with complex structures, near isotropy of the CTE is desirable. By a unique combination of first-principles calculations and neutron diffraction experiments, we identified a significant decrease of CTE anisotropy as the crystal structure of Mo-Si alloys is changed from $D8_m$ (T1 phase) to $D8_l$ (T2 phase). The calculated elastic constants provide insight into the bonding mechanism and form the basis for dislocation modeling. Finally, this investigation points to the increasingly important role of first-principles modeling in alloy designs.

Contact: C. L. Fu, Oak Ridge National Laboratory
Phone: (423) 574-5161, Fax: (423) 574-7659, E-mail: fucl@ornl.gov

Table 1. Elastic constants of Mo_5SiB_2 and Mo_5Si_3

Elastic Constant (GPa)	C_{11}	C_{12}	C_{33}	C_{13}	C_{44}	C_{66}
Mo_5SiB_2 (a=6.027 Å c=10.97 Å)	483	154	419	188	179	127
Mo_5Si_3	438	162	371	136	106	143

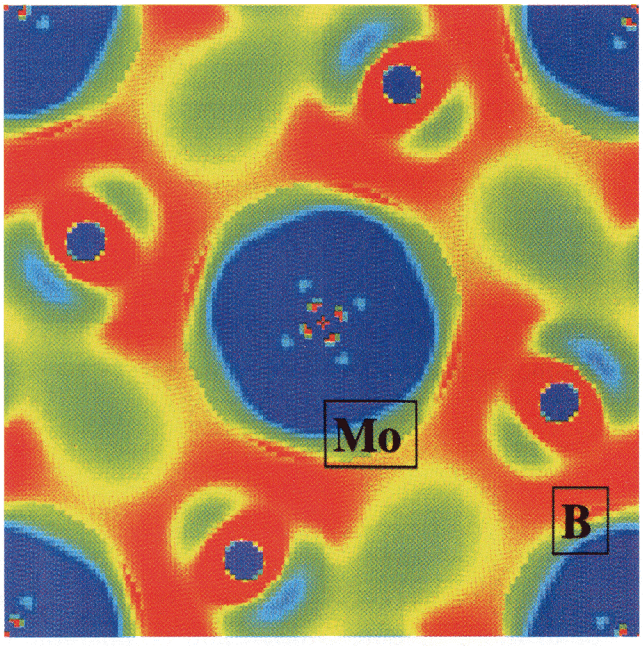

Figure 1. The bonding charge density on the (001) Mo-B plane of Mo_5SiB_2, shows the depletion of density at the Mo sites (denoted by purple color) together with an increase of density in the interstitial region between Mo and B. The bonding has pronounced covalent components (emphasized by red color, which has values larger than $1x10^{-2}$ e/(a.u.)^3).

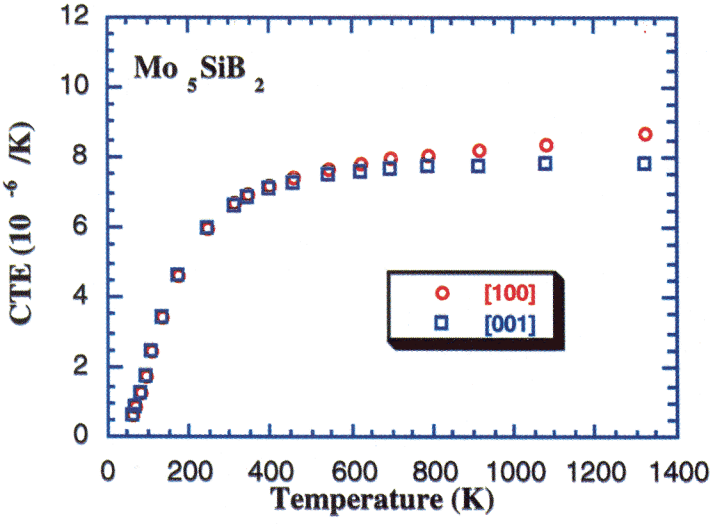

Figure 2. The calculated CTE of Mo_5SiB_2 are nearly isotropic in the [100] and [001] directions.

Effect of Processing on the Mechanical Properties of Mo-Si-B Intermetallics

M. Akinc, M. J. Kramer and Ö. Ünal, Ames Laboratory
J. H. Schneibel, Oak Ridge National Laboratory

Motivation—While boron doped molybdenum silicide alloys containing a large fraction of Mo_5Si_3-B (T1) have shown promising high temperature compressive creep strength and good oxidation resistance, little else is known about these alloys' mechanical properties. Of particular concern are fracture toughness at room temperature and strength and creep behavior at high temperatures. To investigate the effect of composition and processing on the materials' properties of T1-based alloys, a number of different processing routes were investigated. These included powder metallurgical and casting techniques. The strength was measured at temperatures up to 1200°C by three- and four-point flexure methods, and the fracture toughness was determined from flexure tests with chevron-notched specimens.

Accomplishment—Alloy compositions in two different ternary phase fields around the T1 phase were investigated. The first contained T1-MoB-$MoSi_2$ (A1) and the other T1-Mo_5B_2Si-Mo_3Si (A2). The samples were processed either from elemental powders or from fine-grained material produced by self-heating synthesis (SHS). Figure 1 shows that the fracture strength of both alloys increases with temperature. High values on the order of 700 MPa are obtained. The brittle-to-ductile-transition-temperature (BDTT) for alloys A1 and A2 appears to be between 1000-1100°C and over 1200°C, respectively. Macroscopically, alloy A2 fractures in a brittle manner at 1200°C while alloy A1 experiences extensive deformation. Consistent with this, TEM examination of deformed specimens showed that the MoB phase contained defects indicating the presence of plastic deformation. The fracture strengths of cast T1-Mo_5B_2Si-Mo_3Si materials tended to be lower than those of the powder-processed materials.[1] This may be due to the much coarser microstructures (increased flaw sizes) and the microcracking due to thermal expansion anisotropy commonly observed in cast materials. Figure 2 shows the fracture toughness values of the PM alloys. At 1200°C, values ranging typically from 4-6 Mpa$\sqrt{m}$ are observed. Although the A1 material shows ductility at 1200°C, its fracture toughness is not higher than that of the A2 material. The elastic moduli correspond well to values calculated from theoretical results[2] obtained in another part of this Center project.

Significance—This research provides data on important mechanical properties, as well as a qualitative understanding, of ultra-high temperature molybdenum silicide alloys. The high-temperature strengths of these alloys are superior to those of pure $MoSi_2$, and comparable to those of advanced ceramics such as SiC and Si_3N_4. The fracture toughness, while substantially lower than that of current Ni based superalloys, is comparable to that of SiC and Si_3N_4. Future work will continue on understanding the mechanisms of deformation and fracture in these materials.

---

[1] J. H. Schneibel, C. T. Liu, L. Heatherly and M. J. Kramer, Scripta Met. **38**, 1169-1176, 1998

[2] C. L. Fu, Xindong Wang, Y. Y. Ye and K. M. Ho, Intermetallics, **7**, 1-6, 1998

Contact: Matthew J. Kramer, Ames Laboratory
Phone: (515) 294-0276, Fax: (515) 294-4291, E-mail: mjkramer@ameslab.gov

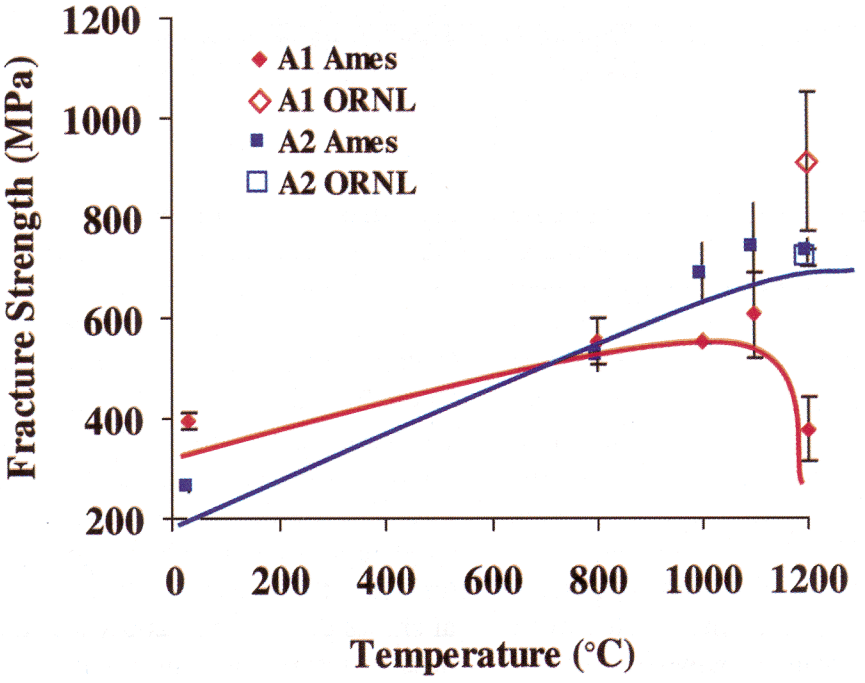

Figure 1. Fracture strength for two different Mo-Si-B alloys as a function of temperature. Closed symbols are for 4 point bend tests and open ones for 3 point bend tests.

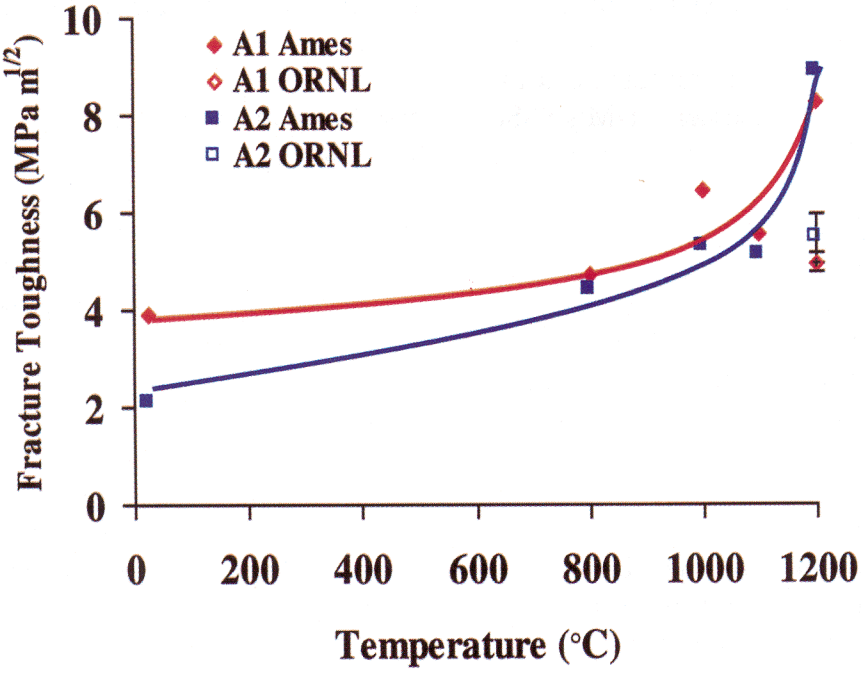

Figure 2. Fracture toughness for two different Mo-Si-B alloys as a function of temperature.

Synthesis and Properties of Al- and B-Modified Mo_5Si_3 Alloys

F. Chu and D. J. Thoma, Los Alamos National Laboratory

Motivation—Evaluations of high-temperature structural properties need insightful interpretations of candidate systems, but development activities require fundamental investigations of alloying behavior. Alloying, incorporation of ductile phases, and microstructural control are most likely required to achieve suitable engineering properties. For example, despite the attributes of Mo_5Si_3, it has limited oxidation resistance from 800°C to 1500°C, limited ambient temperature deformability, and significant thermal expansion anisotropy. However, microalloying with boron increases the oxidation resistance through the formation of a protective borosilicate glass. Therefore, our goal is to understand the alloying behavior and resultant properties of Mo_5Si_3-base alloys. Additions of A1 and B have been explored.

Accomplishment—X-ray powder diffraction experiments of $Mo_5(Si,Al)_3$ (Al: 1 - 10 at. %), annealed at 1200°C for 100 h, revealed that (a) macro-alloying with Al does not change the crystal structure of Mo_5Si_3, (b) the solubility of Al can reach more than 7 at. %, (c) the lattice parameters of $Mo_5(Si,Al)_3$ increases with increasing Al contents in an approximately linear fashion, and (d) $Mo_5(Si,Al)_3$ grain boundary cracking is gradually improved with increasing Al contents, indicating that thermal expansion anisotropy of $Mo_5(Si,Al)_3$ is improved with Al macroalloying.

For Mo_5SiB_2, x-ray powder diffraction experiments revealed ~95% of the T2 phase. Metallography studies demonstrate that the grain boundary cracking problem is virtually eliminated, indicating that the anisotropy of the thermal expansion in the T2 phases is much less than that of the T1 phase in agreement with theoretical calculations (see Brief by Fu et al). The isotropic elastic moduli of the T1 and T2 phases are given in Table 1. Room temperature Vickers indentation tests on the matrix of the Mo_5SiB_2 alloys reveal that the hardness of the T2 phase is around 1600 kg/mm^2 and the fracture toughness is above 3.2 MPa $\sqrt{m}$. Therefore, both the hardness and the fracture toughness of the T2 phase are 30% higher than for the T1 phase. Transmission electron microscopy of the as-grown and annealed Mo_5SiB_2 alloys revealed that there are numerous dislocations in the T2 phase, including dislocations in the matrix as well as grain boundary dislocations, as shown in Fig. 1. However, there is virtually no observable dislocations in T1 Mo_5Si_3.

Significance—The large A1 addition to the Mo_5Si_3-based T1 phase can be understood in terms of the electronic structure of T1 Mo_5Si_3 obtained by Fu et al in this project. It is generally believed that a reduction in the electron density-of-states (DOS) at the Fermi level contributes to the stability of a given structure. The DOS plot of T1 Mo_5Si_3 obtained by Fu et al. indicates that A1 which has one less valence electron than Si, would result in a smaller DOS stabilizing the structure. We believe that stronger metallic bonding may result from A1 alloying and A1 substitution on Si sites, so that the anharmonicity of interatomic bonding in these alloys is reduced For B additions stabilizing the T2 phase, this phase appears to have extremely desirable properties, warranting significant focus upon single crystals and further properties.

Contact: Dan J. Thoma, Los Alamos National Laboratory
Phone: (505) 665-3645, Fax: (505) 665-0657, E-mail: thoma@lanl.gov

Table I The isotropic elastic moduli of the T1 and T2 phases

Phase	B (GPa)	G (GPa)	E (GPa)	ν
T1 Mo_5Si_3	242	126	323	0.278
T2 Mo_5SiB_2	254	143	361	0.263

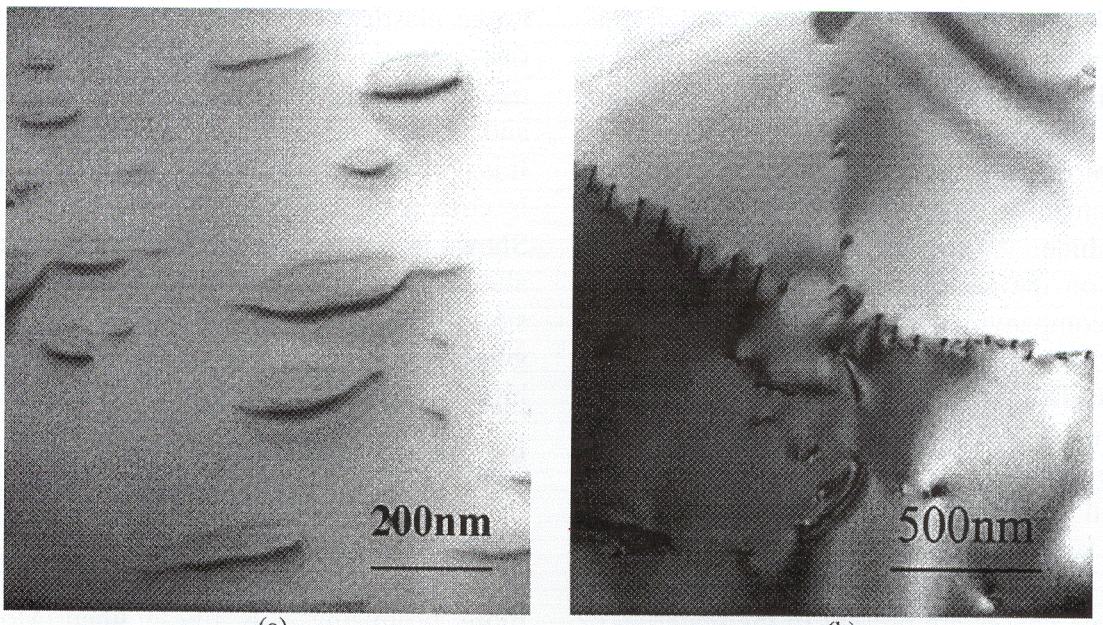

(a) (b)

Figure 1. Dislocations in the T2 phase: (a) ordinary dislocations and (b) grain boundary dislocations.

High Temperature Deformation of Advanced Silicides

T. G. Nieh, J. G. Wang, and L. M. Hsiung, Lawrence Livermore National Laboratory

Motivation—Mo_5Si_3 is the most refractory compound in the Mo-Si binary system with a melting point of 2180°C and a homogeneity range of 2.5 at. % silicon. It possesses good creep resistance at high temperatures, but has a poor oxidation resistance. However, the oxidation properties of Mo_5Si_3 can be substantially improved by adding boron. Considerable efforts have thus been devoted to the study of the Mo-Si-B system. The T2 phase-based, multiphase, molybdenum boron silicide alloys appear to be the most attractive, because ductile Mo particles present in the alloys are expected to offer proper toughening. The high-temperature deformation behavior of these high-temperature alloys as a function of microstructure needs to be characterized. An understanding of the deformation behavior would also provide guidelines for high temperature forming since silicides are difficult to machine. This work complements other efforts on the Mo-Si-B system in this project (see accompanying Briefs).

Accomplishment—T2 is a ternary intermetallic compound Mo_5SiB_2, with a tetragonal $D8_1$ structure (tI32). Polycrystalline Mo_5SiB_2 was received from LANL. The material was arc-melted and then annealed at 1200°C for 100 hours. The X-ray diffraction pattern indicates that three phases are present in the material-T2 phase (Mo_5SiB_2), Mo_3Si, and an unknown phase. The material was tested in compression at 1400°C to a strain of about 10%. The microstructures of both the as-annealed and compressed samples were examined using TEM. In both samples, dislocations were primarily observed in the Mo_3Si phase, and were determined to be <100> dislocations (Figure 1). A high density of stacking faults was also observed in the unknown phase which appears to be the softest. No dislocation was observed in the T2 phase in the annealed sample. Very few dislocations were observed in the T2 phase in the compressed sample (Figure 2). These dislocations are determined to be <100>(001). We also received a powder metallurgy (PM) Mo-9.4Si-13.8B alloy containing T2, Mo_3Si and α-Mo phases from ORNL. The alloy has a fine-grained structure. Tensile tests were conducted with this alloy at 1400 and 1450°C. Large plasticity (~100%) was observed in this fine-grained, PM Mo-9.4Si-13.8B alloy. The true stress-true strain curve obtained at 1450°C and a strain rate of 10^{-4} s^{-1} is shown in Figure 3. It is pointed out that the ultimate tensile strength is comparable to some tungsten-based alloys. Shown in Figure 4 is the fracture surface of the alloy deformed at 1400°C and strain rate of 10^{-4} s^{-1}. The fine-grain appearance suggests the good microstructural stability of the alloy at high temperatures.

Significance—Single-phase Mo_5Si_3 is very strong and not deformable even at elevated temperatures (~1500°C). In contrast, the T2 (Mo_5SiB_2)-based, three-phase alloy is much more promising. A fine-grained Mo-9.4Si-13.8B alloy produced by powder metallurgy methods exhibited high strength of about 140MPa at a strain rate of 10^{-4} s^{-1}; this is comparable to the strength of some tungsten-based alloys. Despite the high strength, the alloy also showed extensive plasticity at temperatures above 1400°C.

Contact: T. G. Nieh, Lawrence Livermore National Laboratory
Phone: (925) 423-9802, Fax: (925) 423-8034, E-mail: nieh1@llnl.gov

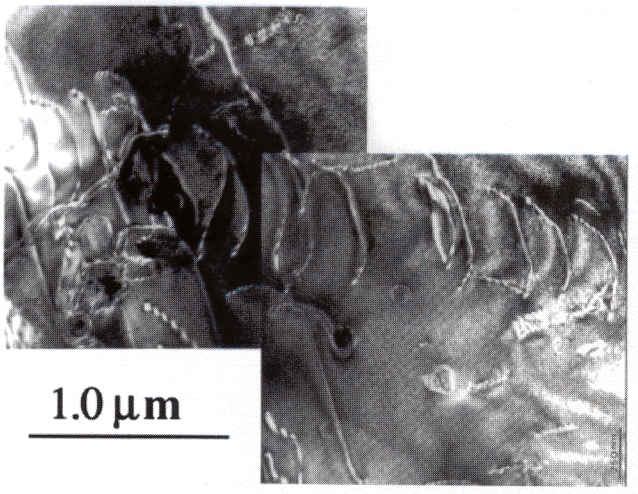

Figure 1. <010>{100} dislocation in a Mo_3Si grain of the T2 - based alloy

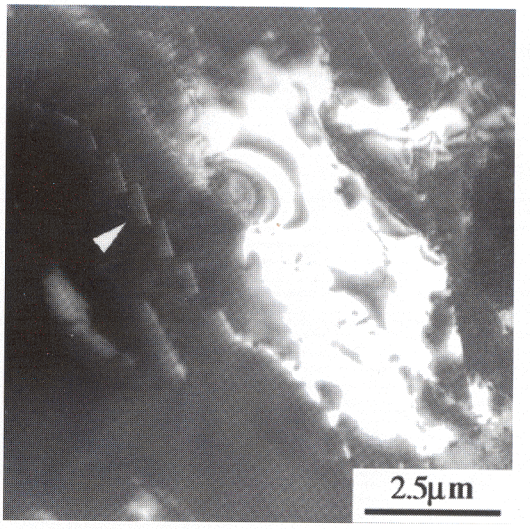

Figure 2. [010](001) dislocations in a Mo_5SiB_2 grain of a deformed T2-based alloy.

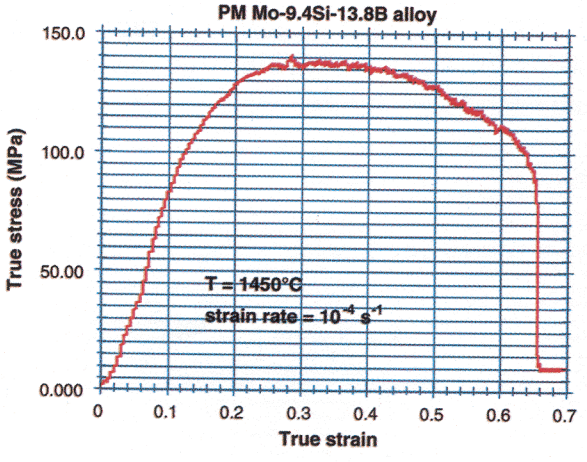

Figure 3. True stress-true strain curve of the Mo-9.4Si-13.8B alloy deformed at 1450°C and a strain rate of $10^{-4}s^{-1}$.

Figure 4. Fracture morphology of PM Mo-9.4Si-13.8B alloy deformed at 1400°C and strain rate of $10^{-4}s^{-1}$.

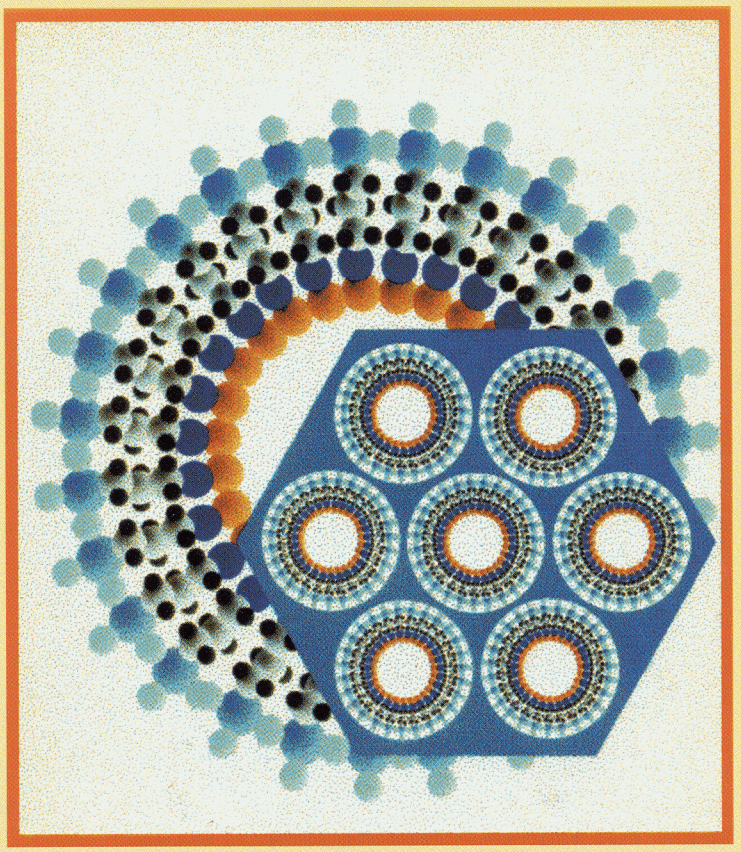

The figures on the front and back covers relate to some of the accomplishments described in this issue of Research Briefs. The above figure shows a schematic drawing of a functionalized mesoporous composite material showing the ordered molecular interface at the pore wall surface. The figure on the front shows a simulation of the positron wave function localized by dangling bonds in hydrogenated amorphous silicon (a-Si:H). This material is a strong candidate for low-cost solar cells, but its electronic properties are degraded by a Si dangling bond defect that traps electrons. Positron annihilation gives information about the location and charge of the defect.

SAND99-1155: Prepared by the DOE Center of Excellence for the Synthesis and Processing of Advanced Materials at Sandia National Laboratories, Albuquerque, New Mexico 87185 for the Division of Materials Sciences, Office of Basic Energy Sciences, U.S. Department of Energy. Sandia is a multiprogram laboratory operated by Sandia Corporation, A Lockheed Martin Company, for the Department of Energy under Contract No. DE-AC04-94AL85000.

Printed in May 1999